

Deep inside a neoproterozoic intra-oceanic arc: growth, differentiation and exhumation of the Amalaoulaou complex (Gourma, Mali)

Julien Berger · Renaud Caby · Jean-Paul Liégeois ·
Jean-Claude C. Mercier · Daniel Demaiffe

Received: 17 June 2010 / Accepted: 4 March 2011 / Published online: 20 March 2011
© Springer-Verlag 2011

Abstract We show here that the Amalaoulaou complex, in the Pan-African belt of West Africa (Gourma, Mali), corresponds to the lower and middle sections of a Neoproterozoic intra-oceanic arc. This complex records a 90–130-Ma-long evolution of magmatic inputs and differentiation above a subducting oceanic slab. Early c. 793 Ma-old metagabbros crystallised at lower crustal or uppermost mantle depths (25–30 km) and have geochemical characteristic of high-alumina basalts extracted from a depleted mantle source slightly enriched by slab-derived sedimentary components ($(\text{La}/\text{Sm})_{\text{N}} < 1$; $\varepsilon_{\text{Nd}}: +5.4\text{--}6.2$; $^{87}\text{Sr}/^{86}\text{Sr}: 0.7027\text{--}0.7029$). In response to crustal thickening,

these mafic rocks were recrystallised into garnet-granulites (850–1,000°C; 10–12 kbar) and subject to local dehydration–melting reactions, forming trondjemite leucosomes with garnet–clinopyroxene–rutile residues. Slightly after the granulitic event, the arc root was subject to strong HT shearing during partial exhumation (detachment faults/rifting or thrusting), coeval with the emplacement of spinel- and garnet-pyroxenite dykes crystallised from a high-Mg andesitic parental magma. Quartz and hornblende-gabbros (700–660 Ma) with composition typical of hydrous volcanic rocks from mature arcs ($(\text{La}/\text{Sm})_{\text{N}}: 0.9\text{--}1.8$; $\varepsilon_{\text{Nd}}: +4.6$ to $+5.2$; $^{87}\text{Sr}/^{86}\text{Sr}: 0.7028\text{--}0.7031$) were subsequently emplaced at mid-arc crust levels (~15 km). Trace element and isotopic data indicate that magmas tapped a depleted mantle source significantly more enriched in oceanic sedimentary components (0.2%). Exhumation occurred either in two stages (700–660 and 623 Ma) or in one stage (623 Ma) with a final exhumation of the arc root along cold P-T path (550°C, 6–9 kbar; epidote–amphibolite and greenschist facies conditions) during the main Pan-African collision event (620–580 Ma). The composition of magmas forming the Cryogenian Amalaoulaou arc and the processes leading to intra-arc differentiation are strikingly comparable to those observed in the deep section of exposed Mesozoic oceanic arcs, namely the Kohistan and Talkeetna complex. This evolution of the Amalaoulaou oceanic arc and its accretion towards the West African craton belong to the life and closure of the Pharusian Ocean that eventually led to the formation of the Greater Gondwana supercontinent, a similar story having occurred on the other side of the Sahara with the Mozambique Ocean.

Julien Berger Chargé de recherches du F.R.S.-FNRS.

Communicated by J. Touret.

Electronic supplementary material The online version of this article (doi:[10.1007/s00410-011-0624-5](https://doi.org/10.1007/s00410-011-0624-5)) contains supplementary material, which is available to authorized users.

J. Berger (✉) · D. Demaiffe
Département des Sciences de la Terre et de l'Environnement,
Université libre de Bruxelles (U.L.B.), GIGC, CP 160/02, av.
F. Roosevelt 50, 1050 Bruxelles, Belgium
e-mail: juberger@ulb.ac.be

R. Cabay
Université de Montpellier2, Géosciences Montpellier, UMR
CNRS 5243, Place E. Bataillon, 34095 Montpellier-cedex,
France

J.-P. Liégeois
Isotope Geology, Royal Museum for Central Africa,
3080 Tervuren, Belgium

J.-C. C. Mercier
Université de la Rochelle, LIENSs, UMR CNRS 6250, ILE, 2
rue Olympe de Gouges, 17042 La Rochelle-cedex 1, France

Keywords Neoproterozoic · Intra-oceanic arc · Gourma · Pan-African · Granulites

Introduction

Island arcs are important geological objects because of their probable contribution to the formation and growth of continental crust since Archean times (Taylor and McLennan 1985; Rudnick 1995). If the shallow sections of intra-oceanic arcs are well known, the structure and the magmatic/metamorphic processes in arc roots are more mysterious due to the rarity of exposures. The deep structure of active arcs is grossly approximated using geochemical tools combined with information brought by lower crustal xenoliths. These studies show that the root of mature island arcs includes dense residual or cumulate mafic to ultramafic rocks with seismic velocities that approach upper mantle values (Moore et al. 1991; Suyehiro et al. 1996; Holbrook et al. 1999; Takahashi et al. 2008; Tatsumi et al. 2008). However, they give little information on the relative proportions of the different constituents and their modes of formation (ultramafic to mafic cumulates or mafic chilled melts, residual garnet-bearing or garnet-free material?). Such information has been acquired on the rare exhumed intra-oceanic arc roots, such as the Kohistan complex (Miller and Christensen 1994) or the Tonsina complex (Debari and Coleman 1989), which are all Mesozoic in age. Their representativeness for all of earth history can therefore be questioned.

The lithologies of the deep parts of island arcs and the petrogenetic processes at their origin are also crucial for the understanding of mantle composition: the inferred high density of the arc root rocks allows them to sink back into the mantle (Kay and Kay 1988; Jull and Kelemen 2001; Behn and Kelemen 2006). Delamination of lower arc crust would refertilise the mantle and may help explain some enriched geochemical end-members in the convecting mantle (Anderson 2005).

This work shows that the Neoproterozoic Amalaoulaou complex in Mali shares many characteristics of the Mesozoic island arc roots, thus representing a rare example of an island arc lower crust formed during the Precambrian Earth. This study thus presents new constraints on the nature and construction of an arc root and overlying middle crust. It moreover brings some new information on the subduction of oceanic lithosphere at the eastern edge of the West African Craton during the Cryogenian.

Previous studies and geological setting

The Amalaoulaou complex is located in the Gourma fold and thrust belt along the eastern Pan-African suture of the West African Craton (WAC) in Mali (Fig. 1). This belt is a pile of thrust sheets that were stacked over the Neoproterozoic sediments of the WAC passive margin (Caby 1979;

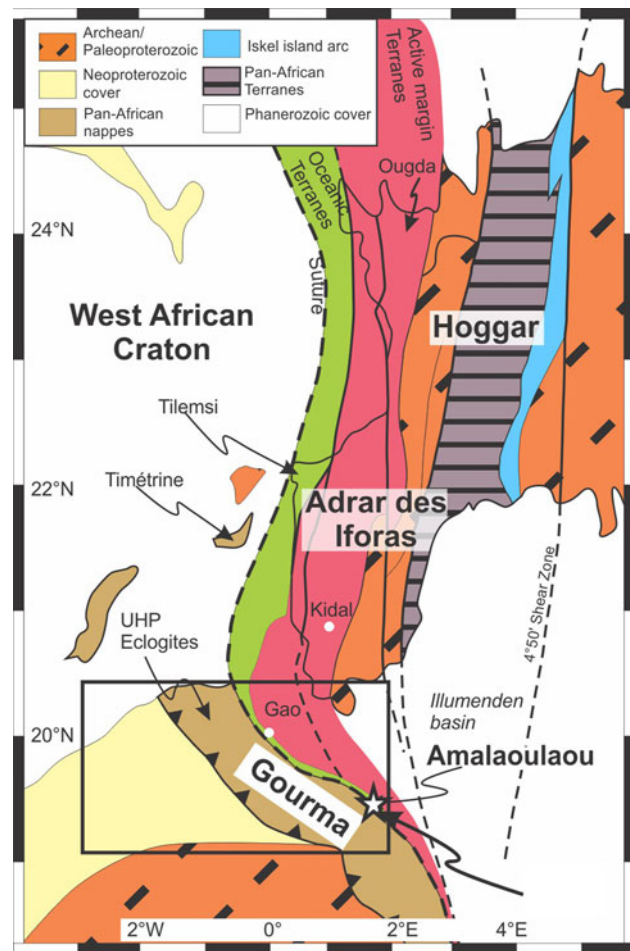
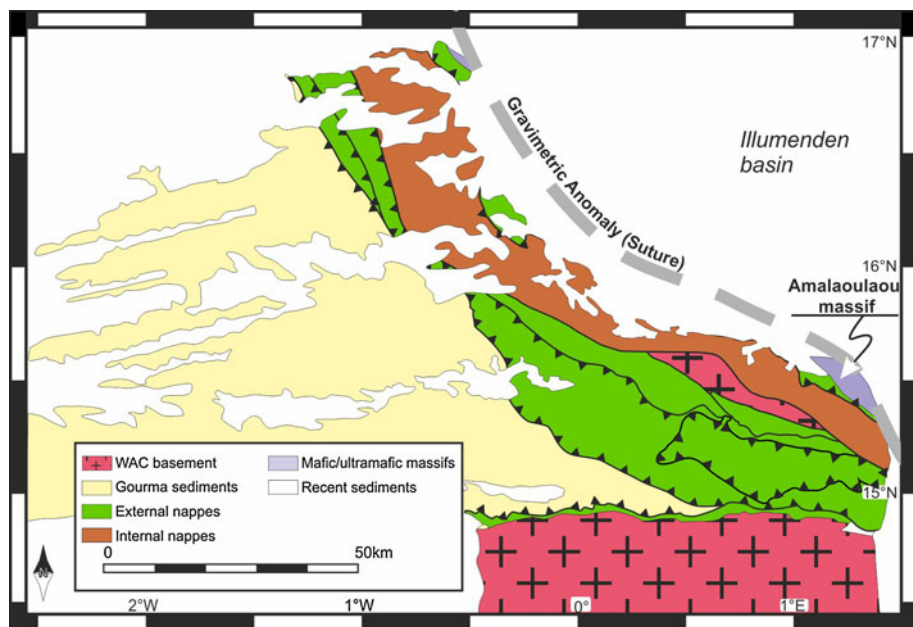


Fig. 1 Schematic map of the Pan-African belt along the eastern border of the West African Craton, showing the position of the main Pan-African outcrops with emphasis on continental and oceanic arcs

Fig. 2). The most external nappes are made of metasedimentary material with an intense imprint of greenschist facies metamorphism and deformation. The internal nappes show relics of high-pressure (HP) to ultra-high-pressure (UHP) metamorphism represented by garnet–phengite–rutile assemblages in metasediments and by coesite-bearing eclogites and blueschists in former magmatic sills and volcano-sedimentary formations (Reichelt 1972; Caby 1979; de la Boisse 1981; Caby 1994; Jahn et al. 2001; Caby et al. 2008). ^{40}Ar – ^{39}Ar dating on phengite from a micaschist equilibrated at UHP conditions has given an age of 623 Ma (Jahn et al. 2001). To the south, in Togo and Benin, subsequent nappe stacking induced by continuing continental convergence started at 610 Ma and lasted until 580 Ma (Attoh et al. 1997). The Amalaoulaou mafic and ultramafic complex was thrust over this whole nappe assemblage at the south-eastern edge of the Gourma belt, and it is partly covered by sediments of the Meso-Cenozoic Illumenden sedimentary basin and recent aeolian sands (Fig. 1).

Fig. 2 Geological sketch of the Gourma fold and thrust belt modified after Buscaill and Caby (2005). Gravity anomaly position is from Bayer and Lesquer (1978)



Reichelt (1972) interpreted the Amalaoulaou rocks as Archean crust on the basis of field and petrographic observations. A further study (de la Boisse 1979) interpreted the Amalaoulaou complex as a granulitised intrusion from the lowermost continental crust, mainly on the basis of whole-rock major element data. Bayer and Lesquer (1978) have shown that the complex is emplaced along a Neoproterozoic suture zone bordering the eastern edge of the WAC. Later studies in the adjacent areas have shown that arc magmatism and relics of subduction zone magmatism and metamorphism are present (Ménot 1980; de la Boisse 1981; Liégeois et al. 1987; Caby et al. 1989). Berger et al. (2009) have shown that garnet-granulites and leucosomes at Amalaoulaou, resembling those in the Kohistan intra-oceanic arc root, are produced by dehydration and dehydration-melting reactions.

The geological map of the Gourma published by Buscaill and Caby (2005) defines the Amalaoulaou structure (Fig. 3). It is a tectonic complex composed of units with different composition and metamorphic features. From bottom to top, the units are (1) serpentinites (former porphyroclastic spinel-harzburgites) associated with Fe-jasper; (2) epidote-amphibolites; (3) sheared metagabbros (protomylonitic garnet-bearing and garnet-free amphibolites) and pyroxenites and (4) quartz-gabbros intruded by small dykes of hornblende-gabbros and tonalitic pegmatites. NW-SE striking foliations in the metagabbro unit and underlying epidote-amphibolite dip to the NE and delineate the axial surface of open to tight recumbent folds.

De la Boisse (1979) provided imprecise ID-TIMS U-Pb zircon ages from three samples of the Amalaoulaou

complex. Available samples and current unsecure conditions in the area preclude generating new U-Pb zircon ages. However, recalculation of the de la Boisse (1979) data using the ISOPLOT software (Ludwig 2003) provides more realistic age constraints. The oldest zircons were extracted from a tonalitic gneiss. This rock was supposed to be genetically linked to the metagabbros by de la Boisse (1979) because it shows a strong amphibolite-facies foliation as in the metagabbro unit. The five grain size fractions poorly define a discordia with an upper intercept of 793 ± 82 Ma (MSWD = 51); three of them are properly aligned (800 ± 9 Ma, MSWD = 0.87), and one zircon fraction is concordant (concordia age = 793 ± 4 Ma, MSWD of concordance = 1.8; Fig. 4). These three ages agree within error limits, and we consider the concordant age of 793 ± 4 Ma as the best age estimation for the crystallisation of magmatic precursors in the metagabbro unit. The four zircons from the quartz-gabbro do not yield satisfactory results with an upper intercept at 707 ± 170 Ma (MSWD = 190). Two zircon fractions are located on the discordia defined by the tonalitic gneiss and could be inherited from that lithology. The two remaining fractions give an upper intercept of 702 ± 7 Ma. One fraction is nearly concordant and gives a $^{207}\text{Pb}/^{206}\text{Pb}$ age of 701 ± 6 Ma (Fig. 4) that we consider as the best age estimate for the intrusion of quartz-gabbro. A late tonalitic pegmatite, intrusive into the quartz-gabbros, defines a two-fraction discordia age of 663 ± 6 Ma; one of these fractions is concordant at 660 ± 4 Ma (MSWD of concordance = 1.8; Fig. 4) that we consider as the best age estimate of these late pegmatitic tonalites. We can conclude that the magmatic activity of the Amalaoulaou island

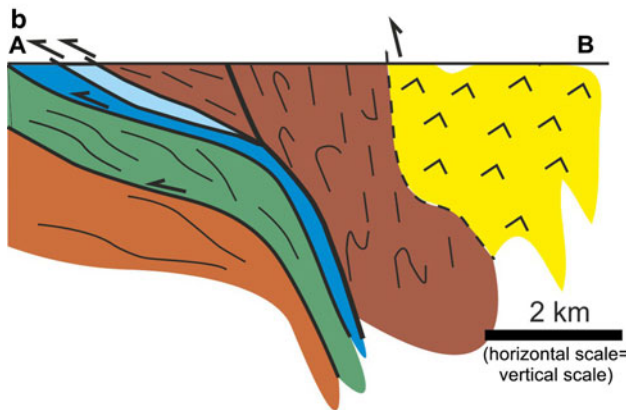
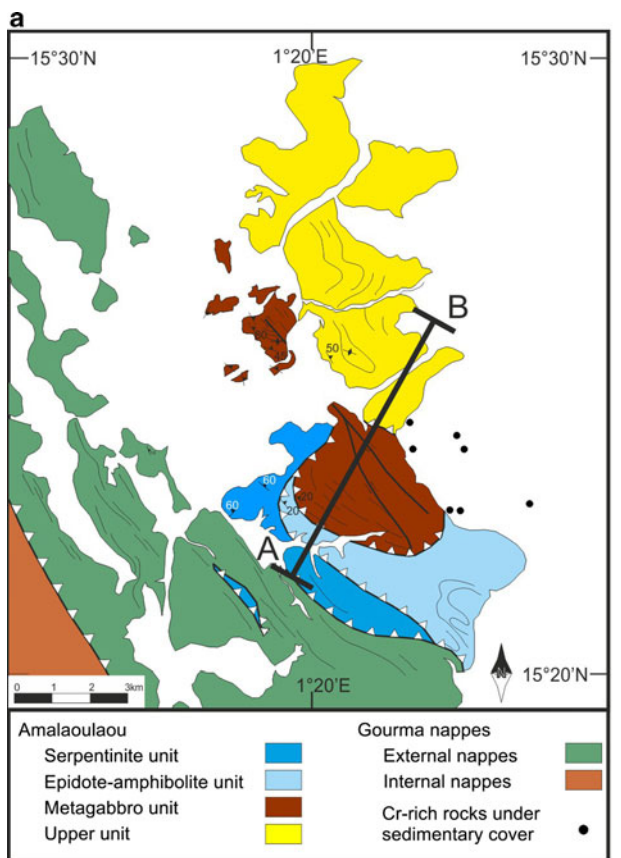


Fig. 3 **a** Geological map of the Amalaoulaou massif modified after Buscail and Caby (2005). The position of Cr-rich (100–1,900 ppm) rocks analysed in the course of surface geochemical prospecting are from Michel Ba (personal communication 2005). **b** schematic cross-section of the Amalaoulaou complex showing the thickness of the four units

arc occurred during the Cryogenian, at least at 793 ± 4 , 701 ± 6 and 660 ± 4 Ma.

Samples description and mineral chemistry

The composition of minerals was measured on Cameca SX50 and SX100 electron microprobes, both at the

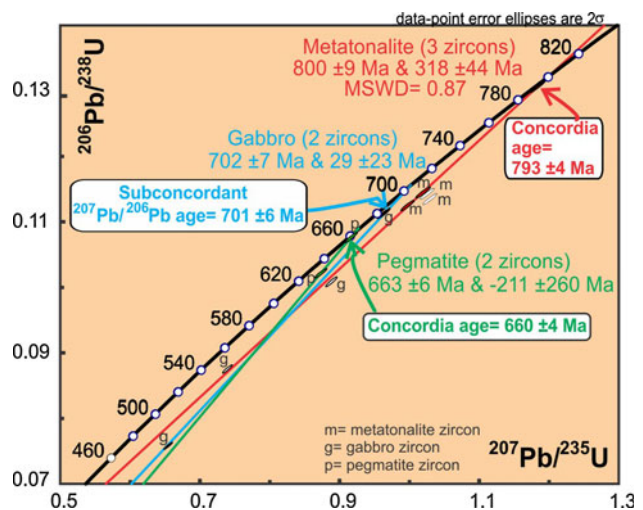


Fig. 4 Concordia diagram with U-Pb zircon ages from de la Boisse (1979) recalculated with Isoplot (Ludwig 2003). Three rocks have been dated: a metatonalite (5 zircons m), a gabbro (4 zircons g) and a pegmatite (two zircons p). Although most zircon fractions are discordant, each rock included concordant or nearly concordant fractions

CAMST (Belgium) and the CAMPARIS (France) services. More details are provided in the Electronic Appendix A1. The tables of mineral compositions are presented in the Electronic Appendix A2.

Serpentinite unit

These rocks are dominated by secondary hydrous phases, namely serpentine-group minerals and chlorite, together with magnetite pseudomorphs after Cr-spinel. Primary anhydrous silicates are lacking, but the dominance of serpentine with the occurrence of some bastite (retrogressed orthopyroxene) suggests that they represent former spinel-harzburgites and dunites. Original high-temperature mantle fabrics are preserved in some boudins of massive serpentinite, defined by elongated sigmoidal porphyroclasts of retrogressed orthopyroxene and needle-like spinel. Submylonitic chlorite schists consist of chlorite and quartz with minor actinolite, white mica and apatite. These could represent altered basaltic dikes. Many Fe-jaspers form contorted lodes cutting across the serpentinites. They consist of quartz, needle-like and granular iron oxides with minor amounts of chlorite and white mica, rare tourmaline, pyrite, carbonates, stilpnomelane and blue amphibole of the winchite group.

Epidote–amphibolite unit

The epidote–amphibolite unit consists of strongly deformed, low-temperature (clinzoisite-bearing) amphibolites (Fig. 6a). They contain small amounts of rutile,

titanite, apatite, retrogressed plagioclase, carbonate, paragonite and quartz. Chloritoid has also been reported by de la Bosse (1979).

Most samples are quartz- and plagioclase-bearing epidote amphibolites (ex: sample 04–75, Table 1) with tschermakite ($Mg\#$: 61–65; Si: 6.2–6.3 a.p.f.u.) and zoisite (X_{Fe} : 0.15–0.16). Two samples (ex: IC 933) have phengite (Si: 6.7–6.8 p.f.u.; $Mg\#$: 55–62) forming 9 vol.% of the rock and show higher proportion of titanite (up to 5%). The amphibole is a blue-green barroisite, and the zoisite is rich in Fe (X_{Fe} : 0.23–0.31). Sample IC 935 contains garnet (Fig. 7; $Alm_{43-52}Grs_{16-20}Prp_{19-35}$) with clinopyroxene inclusions similar to those found in metagabbros and tschermakite ($Mg\#$: 69–72; Si: 6.4–6.7 a.p.f.u.). The ubiquitous association of blue-green amphibole with garnet, zoisite, phengite and chloritoid is indicative of recrystallisation at low-temperature/medium to high-pressure conditions. At the contact with the underlying serpentinite unit, the epidote amphibolites are transformed into mylonitic greenschists consisting of chlorite–actinote–quartz–albite assemblages with accessory muscovite and epidote.

The metagabbro unit

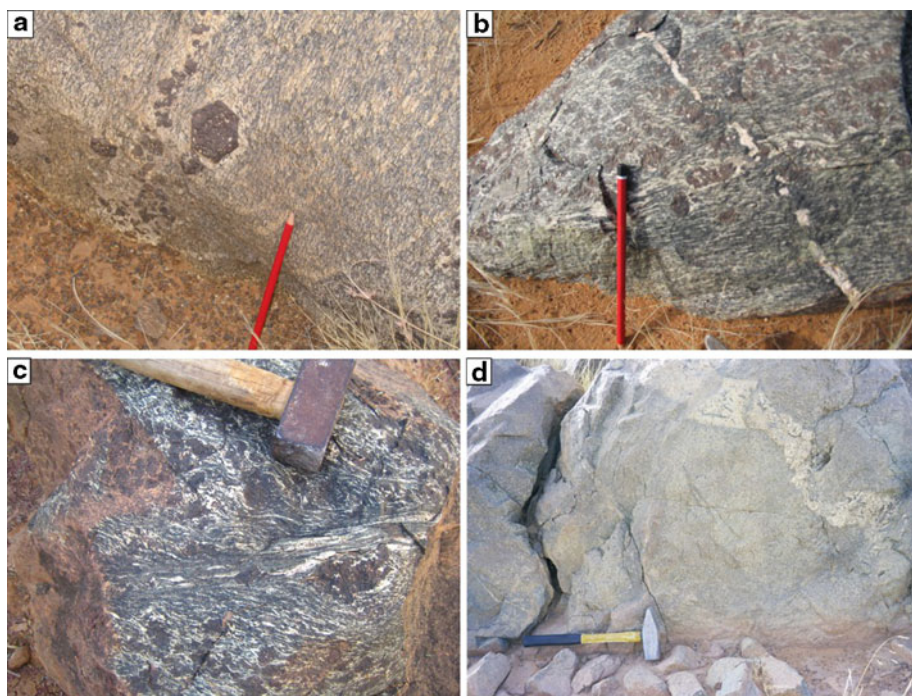
Metagabbro is the dominant lithology in the Amalaoulaou complex. Lenses, layers and dikes of pyroxenites are present within this unit and are described separately. One sample of trondhjemite has been studied.

The metagabbros are plagioclase–clinopyroxene rocks (Table 1) partly overprinted by garnet growth in the granulite-facies conditions and by the development of secondary brown amphibole during an intense phase of shearing. Scarce modal layering from leucogabbros to melagabbros is locally preserved. The most common lithological type is an amphibolite with garnet porphyroclasts in a mylonitic matrix of cpx, amphibole and retrogressed plagioclase. Clinopyroxene (Cpx I), few orthopyroxene grains ($Mg\#: 63\text{--}67$, Al: 0.24–0.44 a.p.f.u.) and very scarce amphibole inclusions (Ti-magnesiohastingsite) are the only relict primary phases (i.e. magmatic or early granulitic). This clinopyroxene (Fig. 6b) is generally coarse-grained (500 μm to 2 mm) and shows the development of mechanical cleavage; it is rich in non-quadrilateral elements (up to 0.45 Al p.f.u., Mg#: 66–75; Fig. 8) compared to the other generation of pyroxenes. Plagioclase is totally replaced by fine-grained epidote–albite–muscovite \pm pyrite \pm barite intergrowths and has not been found as fresh grains. Poikiloblastic garnet (Fig. 6c) is present within leucocratic veins (pl \pm qz \pm hbl) predating the high-temperature (HT) shearing (Fig. 5a) or as sporadic patches associated with plagioclase-rich haloes. Garnet ($Alm_{39\text{--}43}Grs_{10\text{--}18}Prp_{38\text{--}43}$; Fig. 7) encloses rounded clinopyroxene (Cpx II; Mg#: 71–77, Al: 0.22–0.37; Fig. 8),

Table 1 Modal proportion of various rock types sampled at Annalaoulaoua. Calculated V_P and ρ for metababbros and pyroxenites are also given

	04-75	IC 933	IC 935.8	AJB1	AJB14	AJB12	AJB18	AJB25	AJB23	04-73	AJB21	AJB26	AJB28	AJB29	04-92	IC	04-77	IC	04-81	IC 952	IC	04-78	IC 948	
Epidote				Megabro	Megabro	Garnet	Garnet	Garnet	Garnet		Mgabro	Mgabro	Mgabro	Mgabro		936b	944Q	Quartz	Garnet	Plag	Hbl	Trondh-	Tonalite	
Amphib				Amphib	Amphib	Mgabro	Mgabro	Mgabro	Mgabro		Mgabro	Mgabro	Mgabro	Mgabro		Pxite	Pxite	Gabbro	Gabbro	Gabbro	Gabbro	Gabbro	Jemite	
Pl	8	59	53	17	38	26	10	25								14	45	62	64	36	58	49		
Cpx		10	2	21	38	16	49	38		87	63	81	84	91		56	62	49	29					
Opx		4	3							1	1	1	1				21							
Amph	80	85	35	27	42	27		38	7	15	4	10	3											
Grt		25				35	24	20	34	22	1	22	4	1	6	42								20
Scap																		2						
Spinel																								
Fe-Ti																								
Oxide																								
Zoisite	12	6	40																					
Mica		9																						
Qz																								
ρ (at 800°C, 10 kbar)																								
Vp (km/s)		7.0	7.1	7.7		7.2	7.5	7.8	7.5		7.6	7.8	7.7	7.7	7.5	8.0	7.2							30

Fig. 5 Field photographs of the main rock types of the Amalaoulaou massif. **a** Early garnet-bearing leucocratic veins, deformed during the HT amphibolite-facies shearing. **b** Late garnet-free leucocratic vein not deformed by the HT shearing. **c** HT amphibolite-facies centimetre-sized mylonitic oblique shear zone in a garnet metagabbro. **d** Quartz-gabbros intruded by a late (660 Ma-old) tonalitic pegmatite



rutile and scarce plagioclase (Fig. 6c). The mechanisms and P-T conditions of garnet growth are described in detail by Berger et al. (2009).

The garnet-granulites were diversely sheared after the garnet growth. Clinopyroxenes were recrystallised to fine-grained polygonal Cpx III (Figs. 6b and 8; Mg#: 70–80, Al: 0.20–0.35). Strong HT deformation led to the development of protomylonitic textures with local cm-thick ultra-mylonitic bands (Figs. 5c and 6b). Secondary amphibole grew at the expense of clinopyroxene during the HT shearing to form coarse-deformed prophyroclasts that totally replace the pyroxene in some samples. Garnet ($\text{Alm}_{43-46}\text{Grs}_{9-17}\text{Prp}_{34-39}$; Fig. 7) can form pseudo-symplectitic fine-grained intergrowths with clinopyroxene having the most magnesium-rich compositions and low non-quadrilateral element contents (Cpx IV; Mg#: 76–80, 0.15–0.30 Al p.f.u.; Fig. 8). Evidence for late, lower temperature deformation is given by the local development of green magnesiohornblende and chlorite and by the complete replacement of plagioclase by secondary low-temperature assemblage (epidote–albite–white mica \pm pyrite \pm barite). Two generations of leucocratic veins (anorthositic to tonalitic in composition) cut across the metagabbro. The older generation was folded during the HT amphibolitic metamorphism but shows garnet porphyroblasts along the wall of the vein (Fig. 5a). The second generation (Fig. 5b) cut across all metamorphic fabrics (and thus postdate the HT amphibolite event), and garnet has not been observed along the wall of these veins (Table 2).

Pyroxenites crop out as concordant lenses and pods (garnet and plagioclase pyroxenites) or dikes (spinel and garnet pyroxenites) that cut across the main foliation. The dominant lithology is a medium-grained granular spinel pyroxenite (Fig. 6d). Clinopyroxene (80–90 vol.%) is compositionally zoned with core (Mg#: 80–85, Al: 0.27–0.35 a.p.f.u.; Fig. 8) being richer in iron and aluminium than the rim in contact with coronitic garnet (Mg#: 82–87, Al: 0.10–0.18 a.p.f.u.). Spinel (pleonaste with < 1 wt% Cr_2O_3 ; $\text{Mag}_{3-8}\text{Herc}_{29-38}\text{Spl}_{59-67}$) and orthopyroxene (Mg#: 80–87) can together form 15 vol% of the rock. Thin garnet rims surround spinel when it is in contact with pyroxene; the composition of garnet ($\text{Alm}_{30-36}\text{Grs}_{10-16}\text{Prp}_{46-52}$; Fig. 7) is significantly more magnesian than in the garnet metagabbros. In one sample (AJB 26), this coronitic texture has evolved to an equilibrated equigranular medium-grained texture where spinel is present as relic inclusions in garnet. Two other types of pyroxenites have been sampled. (1) An equigranular plagioclase pyroxenite (04–77) containing a low Mg and high Al clinopyroxene (Mg#: 71–74; Al: 0.2–0.5 a.p.f.u.) with 10 vol.% of orthopyroxene (Mg#: 70–72). (2) An equigranular garnet pyroxenite (04–92) forming a dyke cutting across the metagabbros, with garnet porphyroblasts in the vicinity of the dyke. It consists of clinopyroxene (Mg#: 74–80), garnet ($\text{Alm}_{39-44}\text{Grs}_{14-22}\text{Prp}_{36-40}$; Fig. 7) and scapolite grains (close to the calcic meionite end-member), probably replacing a former calcic plagioclase.

Trondhjemite 04–78 is the only felsic vein sampled in the metagabbro unit. It has a dominant equant texture with

Fig. 6 Microphotographs of the main rock types at Amalaoulaou. **a** Epidote amphibolite showing a zoisite porphyroblast. **b** Clinopyroxene porphyroblast (Cpx I) forming a delta object in a ultramylonitic shear band within garnet metagabbros. Recrystallised clinopyroxene (Cpx III) forms the wing of the mantled porphyroblast. The matrix is made of minute clinopyroxene, retrogressed plagioclase and brown amphibole. **c** Garnet porphyroblast enclosing rounded inclusions of Cpx II, plagioclase and rutile in a garnet metagabbro. The matrix is made of retrogressed plagioclase, Cpx II and brown amphibole. **d** Coarse orthopyroxene in an equant spinel clinopyroxenite. **e** Quartz-gabbro showing retrogressed plagioclase, quartz and partly recrystallised clinopyroxene with Fe-Ti oxide exsolution (Schiller plates). **f** Fine-grained hornblende gabbro showing euhedral brown/green amphibole and euhedral retrogressed plagioclase. Other microphotographs of metagabbros and pyroxenites are published in Berger et al. (2009)

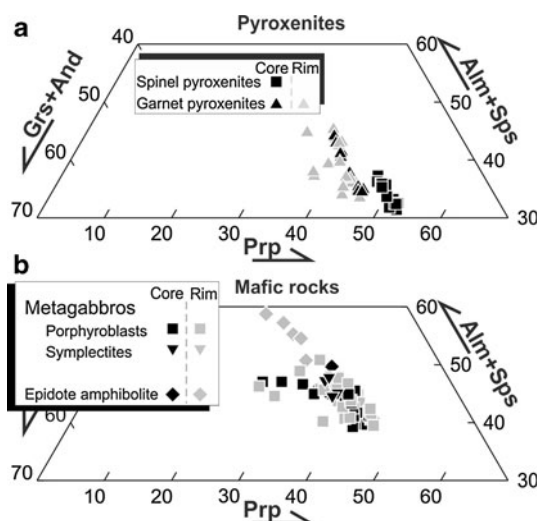
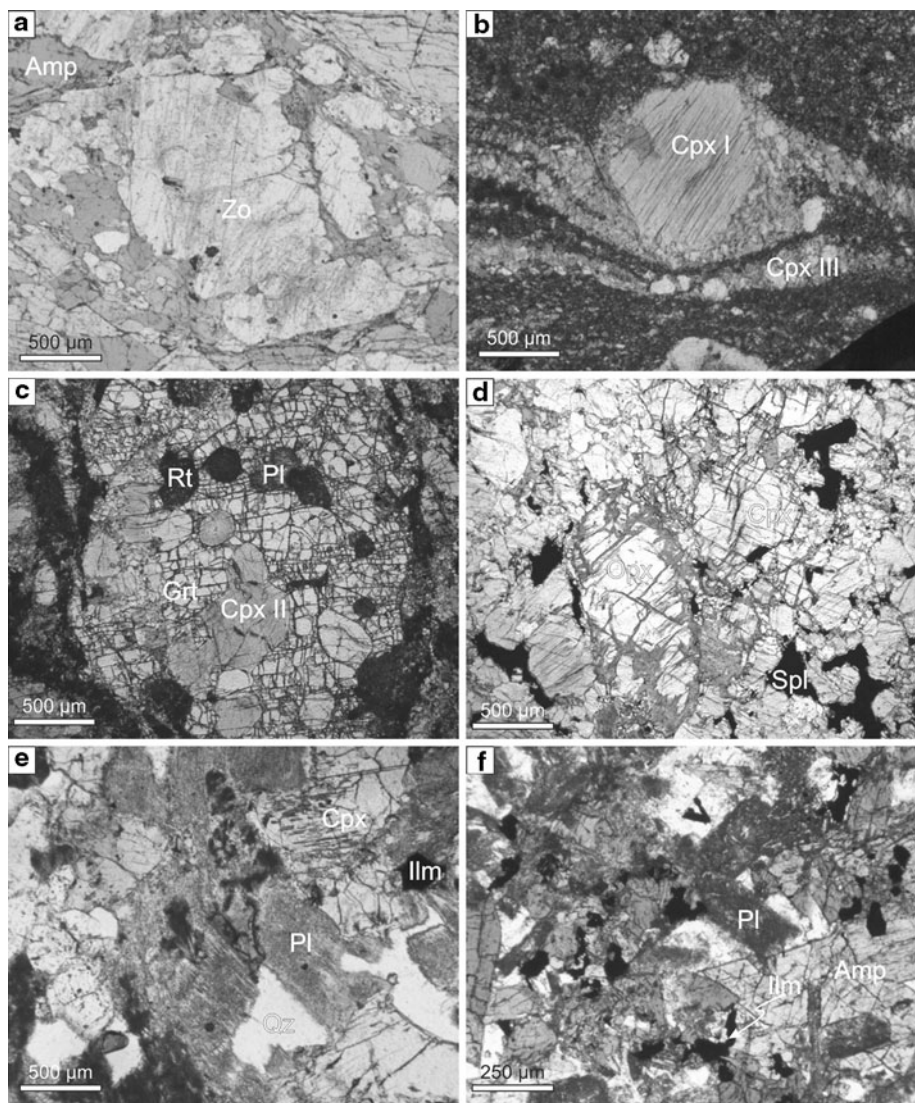


Fig. 7 Composition of garnet in pyroxenites (a), metagabbros and epidote-amphibolites (b) in the Prp-Grs-Alm system

partially preserved plagioclase laths and is made of retrogressed plagioclase, quartz and apatite.

The uppermost unit

This unit is structurally above the metagabbro but is poorly outcropping due to the presence of sand dunes. The main mass of quartz-gabbros is cut across by mafic dykes consisting of fine-grained hornblende-gabbros and by tonalite dykes and pegmatites (Fig. 5d).

Quartz-gabbro is the most common lithology of the upper unit. The primary assemblage is plagioclase, clinopyroxene and quartz with minor apatite, chloritised biotite, ilmenite and accessory zircon (Table 1). The gabbros show an equant equigranular undeformed texture, but Mg-hornblende frequently grew at the rim of clinopyroxene, and plagioclase is totally retrogressed (Fig. 6e). Clinopyroxene has a restricted range of composition with significantly

lower Al, Ti and Na contents (Fig. 8) than metagabbros (Al : 0.09–0.12 a.p.f.u.) but comparable Mg# (68–73).

Tonalites are gneissic amphibole-bearing rocks that consist of cloudy plagioclase, quartz and chloritised green magnesiohornblende with Mn-rich (4–5 wt% MnO) ilmenite grains dispersed in the rock (Table 3).

Hornblende-gabbros have preserved euhedral laths of retrogressed plagioclase and euhedral magnesiohornblende (Mg#: 61–74), pseudobrookite with accessory apatite (Fig. 6f). These textures are of magmatic origin, and the samples do not show evidences for post-magmatic deformation.

Tonalite pegmatites are coarse-grained rocks consisting of retrogressed plagioclase, quartz \pm chlorite, amphibole and apatite. Plagioclase is euhedral, and quartz is interstitial to the feldspar. Chlorite replaces former grains of a Ca-amphibole.

P-T estimates

Magmatic stage

Microprobe analyses of Cpx I cores devoid of exsolution of low-Ca pyroxene is used to constrain magmatic

crystallisation pressures. Clinopyroxene grains used for these estimates are not associated with garnet or orthopyroxene; its composition has thus probably not been affected by chemical reequilibration during the granulite-facies metamorphism. The structural barometer (BA calibration for anhydrous basic magmatic rocks) of Nimis and Ulmer (1998) is useful in this case because it is independent of temperature and the dataset used in the calibration covers whole-rock compositions of the Ama-laoulaou metagabbros. The error on each pressure estimate is about 1.8 kbar. Calculated pressures are in the range 6–12 kbar with most results between 8 and 10 kbar (mean: 9.5 kbar; σ : 1.5 kbar; σ is the standard deviation of the population of computed pressures). The primary magnesiohastingsite (AJB 2) included into Cpx I crystallised around 950–975°C; 8–9 kbar (using amphibole thermometer and barometer of Féménias et al. 2006 and Schmidt 1992, respectively); results are plotted in Fig. 9 (stage A).

In the quartz-gabbro unit, primary amphibole (devoid of rutile exsolution) in hornblende-gabbros has crystallised at 820–840°C. Computed pressures are 4–6 kbar for all rock types with a mean of 5 kbar (σ : 0.5 kbar). Because these samples are undeformed and have locally preserved euhedral plagioclase and amphibole, the temperature obtained

Fig. 8 Composition of pyroxenes in pyroxenites (a) and mafic rocks (b). Compositional fields of pyroxenes from Mesozoic island arc roots are shown for comparison (Kohistan: Jan and Howie 1981; Talkeetna: Greene et al. 2006)

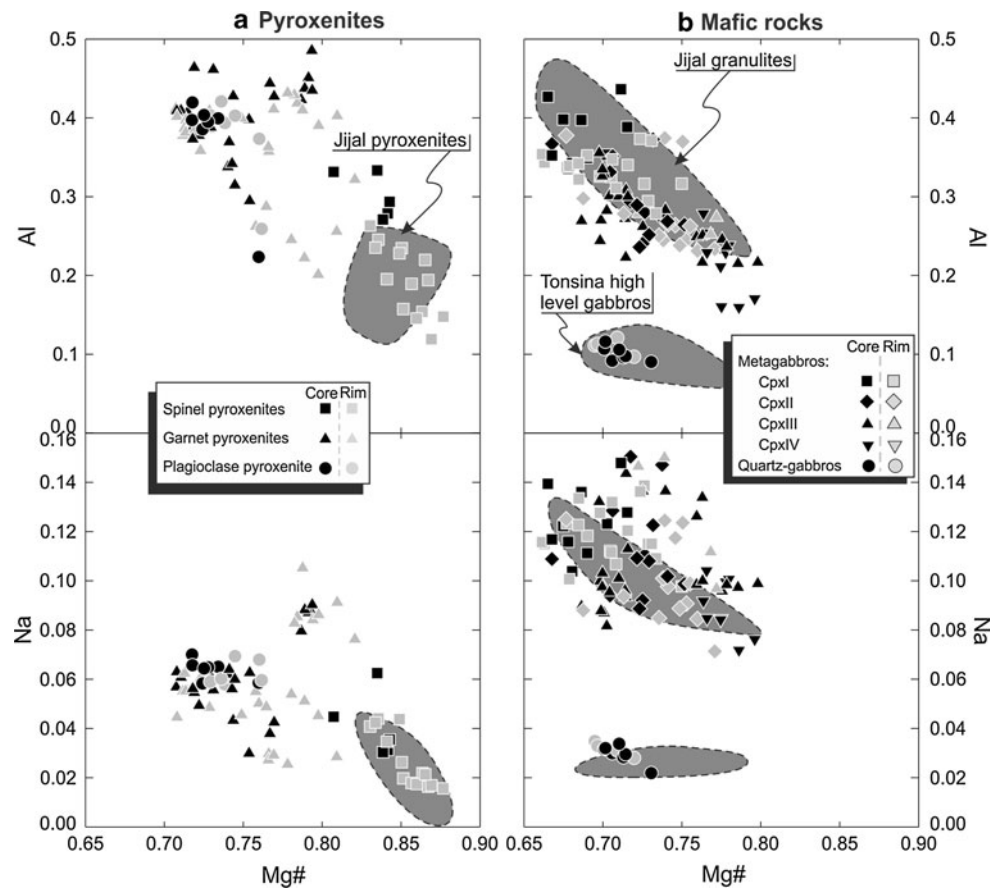


Table 2 Whole-rock major and trace elements analyses of the Amalaoulaou samples

Digestion (wt%)	AJB 1 Acid Mtgabbro	AJB 14 Acid Mtgabbro	04–73 Acid Garnet Mtgabbro	AJB3 Acid Garnet Mtgabbro	AJB12 Acid Garnet Mtgabbro	AJB 18 Acid Garnet Mtgabbro	AJB 25 Acid Garnet Mtgabbro	AJB 23 Acid Garnet Mtgabbro	04–92 Acid Garnet Pxite	AJB26 Acid Garnet Pxite	04–77b Acid Plag Pxite
SiO ₂	46.19	46.96	45.87	44.38	42.87	45.88	45.18	41.89	47.93	40.21	44.49
TiO ₂	1.41	1.01	1.53	1.68	1.06	1.43	1.16	0.73	0.89	1.62	0.64
Al ₂ O ₃	17.57	19.84	17.72	17.75	15.53	16.67	17.44	18.86	9.71	17.90	13.15
Fe ₂ O ₃ t	10.60	9.08	11.65	13.31	12.85	10.66	10.81	10.98	9.11	13.81	11.25
MnO	0.14	0.14	0.20	0.23	0.23	0.16	0.16	0.16	0.12	0.21	0.18
MgO	7.03	5.49	6.89	6.89	11.44	7.69	7.79	10.49	11.58	7.00	13.33
CaO	11.02	10.75	11.77	11.55	11.46	10.71	12.38	13.22	20.33	14.62	15.01
Na ₂ O	3.66	3.66	2.72	2.35	1.76	3.39	2.90	1.43	0.93	1.55	0.74
K ₂ O	0.20	0.13	0.10	0.11	0.15	0.21	0.15	0.34	0.04	0.21	0.07
P ₂ O ₅	0.23	0.18	0.28	0.28	0.08	0.20	0.15			0.14	0.05
LOI	1.47	1.66	0.78	0.75	1.30	2.27	1.25	1.58	0.21	2.19	1.75
Total	99.52	98.90	99.49	99.28	98.73	99.26	99.39	99.66	100.86	99.45	100.67
(ppm)											
Co	54	40	49	54	57	40	47	57	46	43	63
Cr	168	121	148	89	547	158	196	193	600	12	349
Cu	103	60	51	72	22	42	33	50	43	34	200
Ni	65	57	36	25	166	94	30	43	113	24	114
Sc	42	28	45	48	50	37	43	47	66	56	66
Zn	92	66	87	89	89	97	83	77	49	103	56
Rb	0.53	0.68	0.42	1.08	0.45	0.31	1.47	8.62	0.81	0.65	0.57
Sr	446.7	537.3	412.9	381.5	206.5	347.9	370.0	265.7	58.3	950.4	294.2
Yb	22.4	19.5	29.2	31.3	26.1	23.2	18.0	9.5	8.9	40.6	8.1
Zr	104.6	78.6	54.1	62.3	35.1	67.4	79.3	19.0	29.5	78.8	11.3
Zr*			56.6	61.2	30.1	73.5				76.2	11.6
Nb	2.98	2.51	2.84	2.24	1.52	3.70	1.67	0.27	0.13	2.51	0.12
Ba	54.8	55.5	46.3	39.6	83.6	70.9	65.5	60.4	5.7	114.2	12.7
La	3.22	3.37	5.17	3.88	4.74	4.64	2.25	0.47	0.50	3.79	0.99
Ce	10.31	9.01	16.78	13.00	10.80	13.93	7.31	1.62	2.00	13.51	2.91
Pr	2.13	1.72	2.88	2.32	2.11	2.36	1.54	0.39	0.57	2.62	0.51
Nd	12.56	9.78	15.03	12.40	10.47	12.06	9.84	3.03	4.73	14.74	3.06
Eu	1.37	1.08	1.51	1.45	1.14	1.31	1.05	0.50	0.68	1.78	0.48
Sm	3.72	2.84	4.41	3.96	3.02	3.57	2.82	1.25	1.85	4.77	1.16
Gd	4.51	3.50	4.99	4.73	3.60	3.99	3.35	1.64	2.35	5.77	1.47
Dy	4.65	3.80	5.04	5.16	3.83	4.01	3.58	2.05	2.33	6.66	1.53
Ho	0.86	0.70	1.03	1.06	0.83	0.80	0.66	0.38	0.38	1.42	0.31
Er	2.36	1.97	2.91	3.01	2.38	2.22	1.87	1.04	0.94	4.07	0.82
Yb	2.13	1.84	2.74	2.98	2.42	2.12	1.75	0.92	0.66	3.82	0.72
Lu	0.26	0.23	0.41	0.46	0.38	0.32	0.22	0.11	0.07	0.57	0.11
Hf	2.58	1.75	1.73	1.70	0.93	1.85	1.90	0.67	1.12	2.01	0.47
Ta	0.13	0.13	0.16	0.12	0.09	0.23	0.08	0.02	0.05	0.11	0.01
W	2.02	2.99	5.21	4.78	3.07	2.45	2.42	2.30	1.59	1.48	2.37
Pb	0.77	1.33	0.98	0.89	0.61	0.91	0.57	0.24	0.16	3.15	
Th			0.15	0.35	0.07	0.07			0.05	0.21	
U											

Table 2 continued

Digestion (wt%)	AJB21 Acid Spinel Pxite	AJB29 Acid Spinel Pxite	04–75 Alkaline Epidote Amphib	IC 935.8 Alkaline Epidote Amphib	IC 933 Alkaline Epidote Amphib	IC 944Q Alkaline Quartz Gabbro	04–81 Alkaline Quartz Gabbro	IC 944A Alkaline Hbl Gabbro	IC 952 Alkaline Hbl Gabbro	IC 948 Alkaline Tonalite	04–78 Alkaline Trondh- Jemite
SiO ₂	42.27	39.25	41.37	43.58	43.72	49.13	55.20	45.64	49.47	66.30	77.56
TiO ₂	0.57	0.52	1.95	0.44	3.12	0.66	0.60	0.91	1.64	0.37	0.07
Al ₂ O ₃	14.11	17.42	16.87	18.21	12.91	12.74	15.36	14.70	15.07	13.65	13.08
Fe ₂ O ₃ t	9.69	11.25	12.50	11.93	13.67	12.17	8.73	11.28	13.57	6.23	0.64
MnO	0.15	0.16	0.16	0.19	0.18	0.20	0.14	0.18	0.21	0.10	0.01
MgO	15.01	15.34	8.33	8.24	9.02	7.95	5.97	9.50	4.46	1.83	0.23
CaO	17.25	15.55	12.76	13.38	10.26	10.92	8.94	11.38	9.05	5.43	2.32
Na ₂ O	0.58	0.34	2.55	1.32	2.99	1.63	2.68	2.33	2.85	3.68	4.97
K ₂ O	0.02	0.03	0.18	0.15	1.38	0.61	0.38	0.87	0.44	0.16	0.84
P ₂ O ₅	0.03	0.04	0.29		0.98	0.12	0.16	0.05	0.50	0.09	
LOI	0.59	0.71	1.63	1.57	2.02	2.51	2.66	1.91	2.04	1.20	0.71
Total (ppm)	100.27	100.62	98.58	99.02	100.24	98.63	100.81	98.77	99.31	99.06	100.41
Co	75	77	62	44	76	48	35	49	47	440	2
Cr	435	101	182	140	419	269	236	550	18	48	4
Cu	120	96	26	13	52	48	48	512	84	634	17
Ni	298	128	93	62	179	62	48	109	10	365	3
Sc		37	49	23	47	33	41	46	28	1	
Zn	154	201	93	67	123	97	78	89	79	61	12
Rb	0.36		0.58	2.58	62.41	8.48	4.47	12.93	7.33	2.41	12.00
Sr	37.6	28.2	331.1	365.0	557.3	294.3	351.1	286.9	298.3	306.8	340.1
Yb	12.5	22.1	19.0	10.6	23.7	16.4	17.0	14.8	18.2	19.6	1.8
Zr	13.8	7.5	58.8	13.6	134.2	46.0	94.7	40.7	31.7	39.1	31.2
Zr*	14.1	7.5									
Nb	0.07	0.04	4.18	0.03		2.07	2.89	1.89	2.89	1.29	1.84
Ba	2.5	187.9	23.1	17.7	313.5	186.4	183.7	335.1	172.0	95.2	432.9
La	0.92	2.31	3.06	0.38	45.64	5.32	7.86	4.58	3.79	6.27	35.00
Ce	3.23	1.27	10.66	1.45	83.40	11.78	16.52	10.67	8.73	13.97	55.94
Pr	0.63	0.76	2.35	0.42	11.20	1.76	2.31	1.52	1.43	1.95	5.43
Nd	3.81	4.64	15.23	3.65	52.69	9.28	11.54	8.19	8.71	10.28	19.33
Eu	0.56	0.59	1.38	0.59	2.95	0.67	0.79	0.80	1.05	0.68	0.85
Sm	1.50	1.51	4.19	1.29	9.86	2.52	2.79	2.26	2.59	2.60	2.17
Gd	1.98	2.60	4.71	1.77	9.77	2.70	3.09	2.65	3.27	3.13	1.66
Dy	2.23	2.56	4.22	2.14	5.98	3.14	3.22	2.88	3.50	3.44	0.41
Ho	0.46	0.57	0.70	0.40	0.90	0.62	0.61	0.54	0.67	0.69	
Er	1.25	1.56	1.84	1.21	2.17	1.78	1.84	1.59	1.86	2.11	0.16
Yb	1.12	1.20	1.54	1.08	1.41	1.95	1.96	1.61	1.77	2.25	0.15
Lu	0.16	0.17	0.18	0.15	0.15	0.26	0.26	0.19	0.22	0.32	
Hf	0.61	0.40	1.95	0.43	2.19	1.31	2.32	1.24	0.93	0.99	0.75
Ta	0.01			0.02		0.14	0.15	0.11	0.12		0.09
W	3.95	2.19	1.24	2.20	0.95	2.05	2.07	1.07	2.12	6.80	8.62
Pb				0.43	0.75	3.33	2.76	2.56	2.31	1.10	4.49
Th	0.19	0.14	0.01	0.01	6.50	0.31	0.18	0.33	0.42	0.30	1.64
U					1.61	0.14	0.06	0.12	0.15	0.13	0.05

Zr* is the concentration of Zr dosed after an alkaline digestion

Table 3 Sr-Nd isotopic composition of representative Amalaoulaou samples

	$^{87}\text{Rb}/^{86}\text{Sr}$	2σ	$^{87}\text{Sr}/^{86}\text{Sr}$	2σ	$^{87}\text{Sr}/^{86}\text{Sr}$	2σ	$^{87}\text{Sr}/^{86}\text{Sr}$	2σ	$^{147}\text{Sm}/^{144}\text{Nd}$	2σ	$^{143}\text{Nd}/^{144}\text{Nd}$	2σ	ε_{Nd}	ε_{Nd}	T_{DM}	
					660 Ma	730 Ma	800 Ma				660 Ma	730 Ma	800 Ma			Ma
AJB1	Mtgabbro	0.0035	0.0002	0.702892	0.000010	0.70286	0.70285	0.179	0.004	0.512848	0.000008	5.6	5.7	5.9	878	
AJB14	Mtgabbro	0.0036	0.0002	0.702807	0.000010	0.70277	0.70277	0.175	0.004	0.512843	0.000008	5.8	6.0	6.2	818	
04-73	Mtgabbro	0.0029	0.0002	0.702969	0.000008	0.70294	0.70294	0.178	0.004	0.512820	0.000007	5.2	5.3	5.5	952	
AJB12	Mtgabbro	0.0062	0.0004	0.702883	0.000008	0.70282	0.70282	0.174	0.003	0.512797	0.000007	5.0	5.2	5.4	960	
04-77B	Plag Pxite	0.0056	0.0003	0.702893	0.000008	0.70284	0.70284	0.229	0.005	0.513096	0.000010	6.2	5.9	5.6	-4863	
AJB21	Spl Pxite	0.0280	0.0016	0.703007	0.000010	0.70274	0.70272	0.238	0.005	0.513103	0.000009	5.6	5.3	4.9	-9199	
AJB26	Grt Pxite	0.0020	0.0001	0.703387	0.000008	0.70337	0.70336	0.196	0.004	0.512896	0.000007	5.1	5.1	5.1	1229	
IC 952	Hbl gabbro	0.0711	0.0041	0.703896	0.000008	0.70323	0.70316	0.180	0.004	0.512820	0.000005	5.0	5.2	5.3	1002	
IC 944Q	Qz-gabbro	0.0834	0.0048	0.703767	0.000008	0.70298	0.70290	0.164	0.003	0.512719	0.000008	4.3	4.6	4.9	1003	
IC 948	Tonalite	0.0227	0.0013	0.703358	0.000010	0.70314	0.70312	0.153	0.003	0.512682	0.000008	4.6	5.0	5.3	914	
04-78	Trondhjemite	0.1020	0.0059	0.704189	0.000010	0.70323	0.70313	0.068	0.001	0.512271	0.000008	3.7	4.9	6.0	814	

from the composition of magmatic amphiboles is believed to represent late-magmatic conditions (Fig. 9, stage A').

Granulitic stage

The equilibration pressure and temperature of thin garnet coronas around spinel in spinel pyroxenites have been computed using the garnet–orthopyroxene exchange thermometer of Harley (1984a), the two pyroxene thermometer included in the QUILF software (Andersen et al. 1993), and the garnet–orthopyroxene barometer of Harley (1984b). All these calibrations are valid for Fe-rich compositions typical of mafic igneous rocks, and they cover the

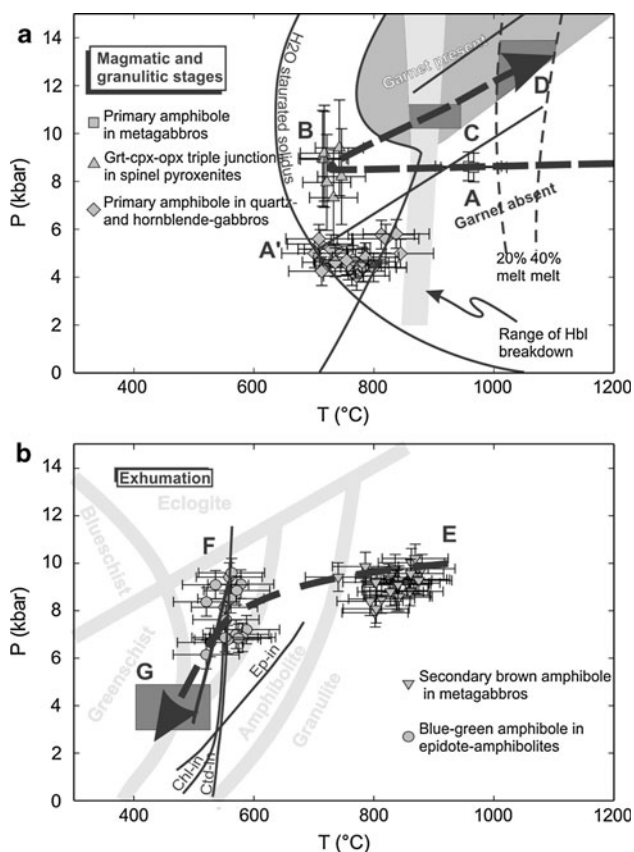


Fig. 9 P-T paths recorded in the Amalaoulaou massif. **a** Magmatic and granulitic stages. **b** Exhumation. Dehydration melting solidus, wet solidus and garnet-present and garnet-absent domains from Lopez and Castro (2001); 20 and 40% melt curves for metabasalt melting from Rapp and Watson (1995); P-T range of hornblende breakdown from Pattison (2003). A and A' magmatic crystallisation of amphibole in different units; B coronitic garnet in pyroxenites and two-pyroxenes equilibrium conditions in the garnet-free metagabbros; C recrystallisation of garnet–spinel pyroxenites and garnet growth by dehydration and dehydration melting in the metagabbros; D melting event generating garnet–clinopyroxene–rutile restites and tonalite; E HT amphibolite stage; F LT exhumation stage; G greenschist overprint

P-T range of equilibration of Amalaoulaou samples. As Fe–Mg exchange reactions continue during cooling (Fitzsimons and Harley 1994), only the maximum P-T conditions will be discussed. Using garnet–orthopyroxene thermobarometry, the average calculated P-T conditions are 725°C (1σ : 20°C) and 6.9 kbar (1σ : 1 kbar). The combination of the two pyroxene thermometer and the garnet–orthopyroxene barometer gives slightly higher P-T values: $750 \pm 27^\circ\text{C}$, 7.7 ± 1.1 kbar. The garnet and spinel pyroxenite AJB 26 is characterised by a more evolved medium-grained isograngular polygonal texture with relics of coronitic garnet; the equilibrium temperature is higher (800–900°C at 10 kbar) for such coarse garnet–clinopyroxene pairs. As orthopyroxene is absent in this sample, the pressure cannot be determined. The opx-free garnet and spinel pyroxenite (AJB 6) with an equigranular texture also has higher T of equilibration for garnet–clinopyroxene pairs compared to coronitic samples (830–875°C). Garnet and scapolite pyroxenites yield equilibrium temperature in the same range: 810–860°C at ca. 10 kbar (Fig. 9, stage C).

Garnet–clinopyroxene thermometry (Ganguly 1979) has been applied to garnet metagabbros, but no independent estimation of pressure is possible in these orthopyroxene-free samples. However, from phase equilibria constraints and taking into account experimental studies on similar bulk-rock composition (Rapp and Watson 1995; Pattison 2003), it is known that garnet is present at $P \geq 10$ kbar for a temperature close to 800–850°C. Garnet–Cpx II equilibration temperatures from garnet metagabbros are significantly higher than those calculated for spinel pyroxenites: 730–900°C with most temperatures above 810°C (calculated at 10 kbar). The presence of garnet–clinopyroxene–rutile restites together with trondhjemite melt depleted in HREE, Y and Ti argues that the P-T path has crossed the dehydration–melting solidus (Rapp and Watson 1995), the P-T conditions were above 800–850°C and 10 kbar during the melting event.

HT amphibolite–granulite stage

In the absence of fresh plagioclase, amphibole–plagioclase thermometers cannot be applied here. Ti in amphibole thermometer and Al in amphibole barometers, even if calibrated for magmatic systems, can be used on available samples, but results will only be semiquantitative. When applied to the amphibole from the metagabbros, temperatures of crystallisation between 725 and 875°C (Féménias et al. 2006) at pressures between 8 and 11 kbar (Schmidt 1992) are obtained (Fig. 9, stage E). Garnet–Cpx III pairs forming symplectite-like textures give significantly lower temperatures (660–720°C for a pressure fixed at 8 kbar) that probably represent conditions of garnet destabilisation.

Epidote–amphibolite stage

The association barroisite–zoisite ± garnet ± white mica in the amphibolite sole is a common paragenesis of the epidote–amphibolite facies. Minor amounts of paragonite and chloritoid constrain temperatures to $< 570^\circ\text{C}$ (Will et al. 1998; Liu and Ye 2004). Pressure cannot be tightly constrained, but the domain occupied by the epidote–amphibolite facies in a P-T grid indicates pressures between 3 and 10 kbar (Will et al. 1998). Using the semiquantitative amphibole thermometer and barometer cited above, the P-T conditions can be fixed between 520 and 570°C and 6 and 9 kbar (Fig. 9, stage f).

Greenschist facies assemblages

The development of chlorite as replacement product of amphibole in some metagabbros and the widespread retrogression of plagioclase into epidote +albite ± white mica ± carbonate ± chlorite ± quartz suggest a ubiquitous metamorphic imprint and/or fluid percolation under LT–LP conditions. Some shear zones in the amphibolite show the association chlorite +quartz +epidote +titanite ± zoisite. Following experimental data (Liou et al. 1985 and references therein), chlorite, epidote and zoisite coexist between 400 and 550°C at 3 ± 2 kbar (Fig. 9, stage G).

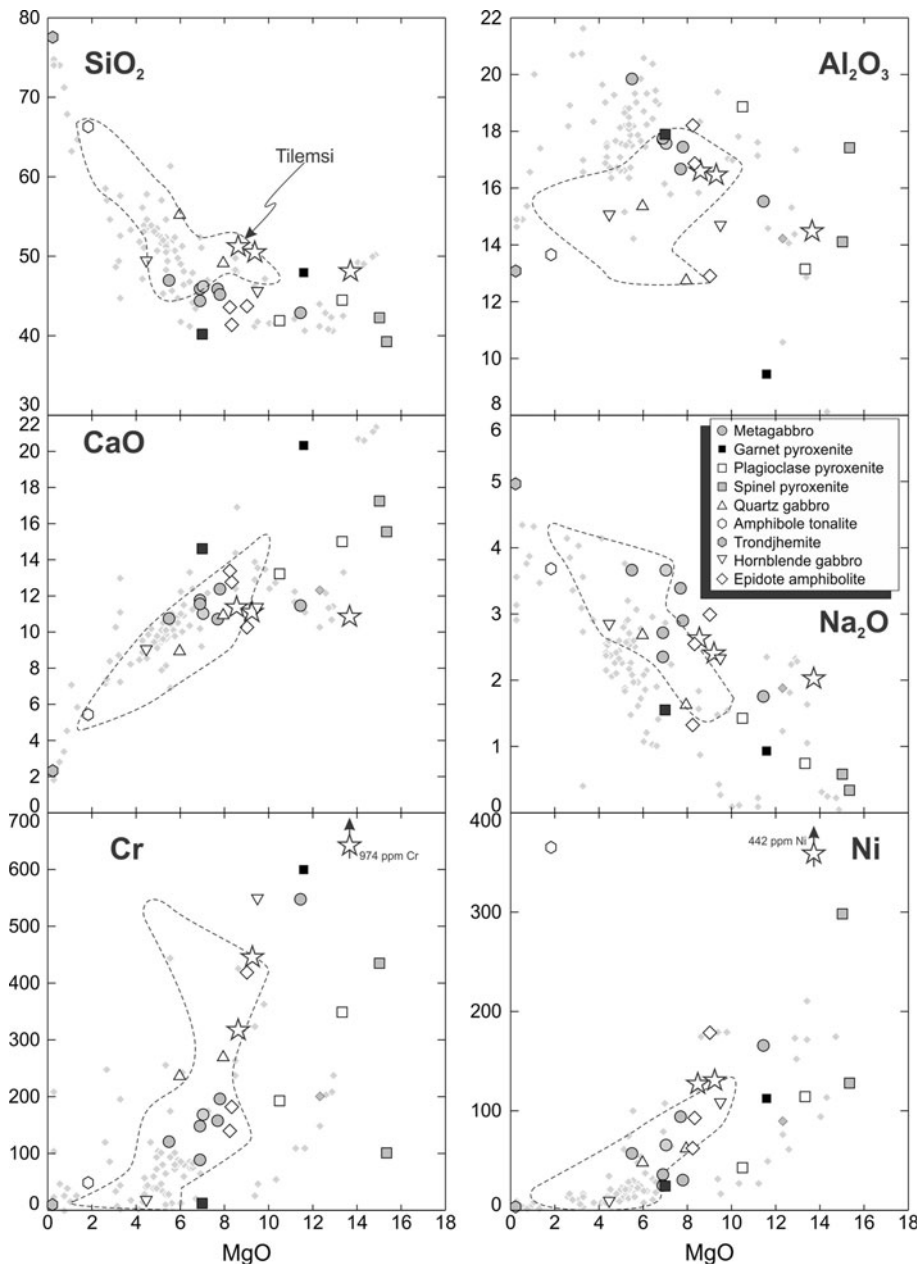
Major and trace elements geochemistry

Major elements were dosed by ICP-AES (Royal Museum for Central Africa, Belgium) using an alkali digestion procedure. Trace elements were dosed by ICP-MS using either an alkali digestion protocol and/or high-pressure HF–HNO₃–HClO₄ acid digestion (Royal Museum for Central Africa, Belgium and Service d'analyse de roches et minéraux, France). More details are provided in the electronic appendix A1.

Metagabbros

Most of metagabbros have similar major and trace element compositions (Figs. 10, 11a and 12a). They have low silica content (45–47 wt%) with a Mg# ranging between 50 and 60 and show compositions matching those of tholeiitic low-silica high-Al basalts, i.e. high Al contents (15–18 wt% Al₂O₃) with low total alkali concentrations (2.5–3 wt%) and rather high Ti contents (1–1.7 oxide wt%). Samples AJB12 and AJB23 have high MgO content (10–11 wt%) with low silica (42–43 wt% SiO₂), which is typical of ferromagnesian mineral cumulates (clinopyroxene and spinel) as evidenced by the high Cr content of these samples (up to 547 ppm instead of 100–200 ppm for other

Fig. 10 Bowen diagrams showing the major and transition elements composition of the Amalaoulaou rocks compared to other Pan-African arc rocks (Tilemsi: Dostal et al. 1994) and continental arcs (Ougda: Dostal et al. 1996) and to peridotites, pyroxenites, websterites, mafic granulites, gabbros and felsic rocks from the Kohistan arc root (*light grey points*; Garrido et al. 2006; Dhuime et al. 2007, 2009). White stars show the composition of most primitive magmas from three representative active oceanic arcs. From the highest MgO content to the lowest: Lesser Antilles, Aleutian and Mariana (Kelemen et al. 2003)



metagabbros). The sample AJB3 is enriched in Al (20 wt% Al_2O_3) and Sr (537 ppm) compared to other metagabbros, probably indicating a significant amount of cumulus plagioclase.

The metagabbros are LREE-depleted ($(\text{La}/\text{Sm})_N$: 0.7–1) and have REE patterns that resemble that of average N-MORB except lower HREE content (Fig. 11a). The absence of Eu anomaly ((Eu/Eu^*) : 0.98–1.05) despite the presence of plagioclase as a major mineral phase strongly suggests that most metagabbros represent chilled melts rather than cumulates.

The multielement diagrams show patterns that are globally around N-MORB values but with some anomalies

(Fig. 12a). Strong positive anomalies are observed for Ba, Rb, Pb and Sr and slight negative anomalies for Nb-Ta ($(\text{Nb}/\text{Nb}^*)_N$: 0.3–0.7) and Zr-Hf. Most HFSE are slightly depleted compared to N-MORB. This is distinctive of the influence of subduction-derived components (either slab-derived fluids or recycled sediments) in the mantle source of the Amalaoulaou metagabbros.

The trondjemite 04–78 has a strongly fractionated REE pattern ($(\text{La}/\text{Yb})_N$: 157; Fig. 11a) but shows the same LILE (except Th), Nb-Ta, Pb and Sr contents as the other basic to intermediate rocks from the upper unit (Fig. 12a). Strong depletion in HREE, Y and Ti led Berger et al. (2009) to propose that the trondjemite was formed by melting of a

Fig. 11 Chondrite-normalised REE patterns for metagabbros (**a**); pyroxenites (**b**); quartz and hornblende-gabbros and tonalites (**c**) and epidote-amphibolite (**d**). N-MORB from Hofmann (1988); Kohistan rocks from Garrido et al. (2006) and Dhuime et al. (2007, 2009); Cretaceous Greater Antilles tholeiites from Marchesi et al. (2007); Talkeetna rocks from Greene et al. (2006). Normalisation values from McDonough and Sun (1995)

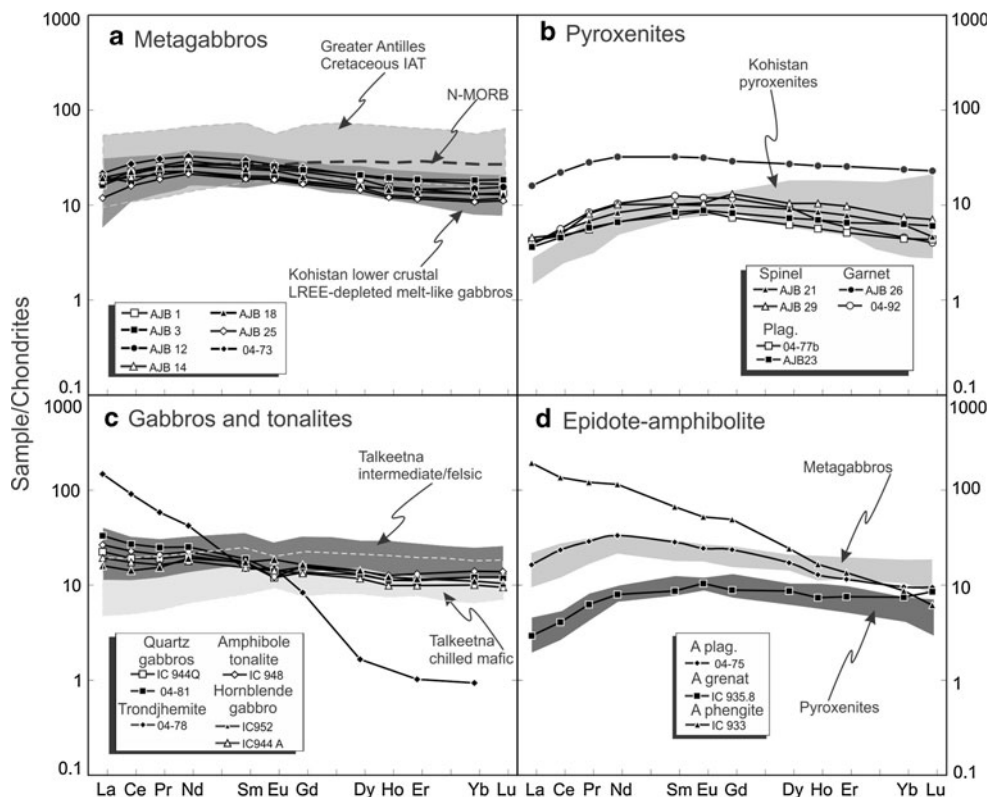
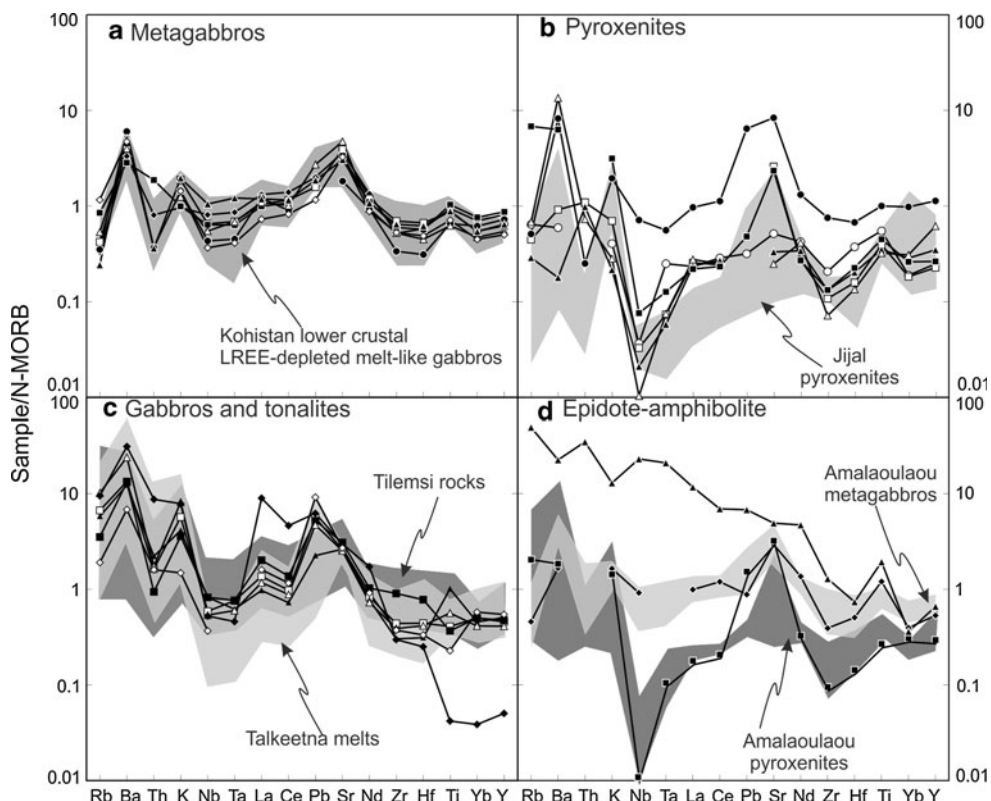


Fig. 12 N-MORB-normalised multi-element diagrams for metagabbros (**a**); pyroxenites (**b**); quartz- and hornblende-gabbros and tonalites (**c**) and epidote-amphibolite (**d**). Same references as previous figure except for the Tilemsi intra-oceanic Pan-African arc (Dostal et al. 1994). Normalisation values from Hofmann (1988)



metagabbro leaving a garnet–clinopyroxene–rutile residue that is locally observed in pseudo-migmatitic samples and in ultramafic lenses within metagabbros.

Pyroxenites

The pyroxenites display high MgO content (12–16 wt%) with low Si, high Ca (14–20 wt% CaO) and Cr–Ni contents (up to 600 and 300 ppm, respectively), the plagioclase-bearing pyroxenite being intermediate in composition between spinel pyroxenites and metagabbros (Fig. 10). The garnet pyroxenites have the lowest MgO content and are generally closer in this regard to metagabbros than to other pyroxenites. Sample AJB 26 is indeed close to the mean composition of metagabbros except for lower content in Si, Cr and Ni but higher Ca content.

Despite variations in modal and major element composition, the trace element contents are surprisingly similar among the different types of pyroxenites. The REE patterns are concave downward with low REE content (between 3 and 10 times the chondritic values; Fig. 11b), a typical pattern for pyroxenites. The multielement distribution is also homogeneous for the different types (Fig. 12b); they all show a strong negative Nb anomaly with a less-pronounced Ta-negative spike (Nb/Ta : 2–8 for the pyroxenites; 11–18 for metagabbros). Some pyroxenites show enrichment in Ba and Sr, the most Sr-rich samples being the plagioclase pyroxenite and one garnet-bearing sample. The high Sr content of sample 04–92 shows that scapolite has probably been formed by plagioclase-consuming reaction.

Upper unit

The rocks forming the uppermost tectonic unit of the Amalaoulaou complex have a wide range of composition, from low-silica high-Mg basic samples to tonalites with high Si, Al and Na (Fig. 10). All samples, however, plot in the field of tholeiitic magmas in AFM or FeO/MgO vs SiO_2 plots. The two analysed quartz-gabbros range between 49 and 56 wt% SiO_2 with 6–8 wt% MgO (Mg#: 56–58). They have lower Al, Ti and Ca contents compared to metagabbros but comparable Na. Hornblende-gabbros have also low silica content (47–50 wt%), but one sample is more primitive as demonstrated by its high Mg content (9 wt% MgO, Mg#: 63) compared to the others (Mg#: 37). The amphibole tonalite has an intermediate composition between the trondhjemite and the quartz-gabbros. The Ni content of the tonalite is abnormally high for such felsic rock (380 ppm), and it is linked to the presence of hydrothermal Ni-sulphides in the secondary assemblages replacing plagioclase.

Despite large variations in major elements, trace element compositions of these samples are quite comparable. They show REE patterns (Fig. 11c) slightly enriched in

LREE ($(\text{La}/\text{Sm})_{\text{N}}$: 0.9–1.8; $(\text{La}/\text{Yb})_{\text{N}}$: 1.4–2.7) with no or only a slight negative Eu anomaly (Eu/Eu^* : 0.73–1.09). Multielement patterns (Fig. 12c) show an enrichment of LILE compared to HFSE with positive spikes in Ba, K and Pb and negative anomalies in Nb–Ta ($(\text{Nb}/\text{Nb}^*)_{\text{N}}$: 0.1–0.3), Th, Zr-Hf.

Epidote amphibolites

Two amphibolites have major element composition very close to the metagabbros and to one plagioclase pyroxenite whereas the phengite-bearing sample (IC933) has low Al and Si content (13 and 43 oxide wt%, respectively; Fig. 10), high alkalis (4.3 wt% $\text{Na}_2\text{O} + \text{K}_2\text{O}$) and TiO_2 (3 wt%). The nature of the protolith of these amphibolites can be easily determined using trace element patterns. The plagioclase amphibolite has similar REE and multielement patterns to the metagabbros while the garnet-bearing amphibolite has similar trace element patterns to the Amalaoulaou pyroxenites (Figs. 11d and 12d). They thus represent samples from the metagabbros unit that underwent low-temperature medium-pressure recrystallisation and deformation in the sole of the Amalaoulaou arc root. However, sample IC933 is richer in REE (6–200 times the chondritic values) with a steep LREE-enriched distribution ($(\text{La}/\text{Yb})_{\text{N}}$: 22). It is strongly enriched in LILE compared to HFSE with small negative anomalies in Ba, K, Zr-Hf and Ti. Such geochemical fingerprints are typical for undersaturated alkaline lavas, such as nephelinites and basanites.

Sr–Nd isotopic compositions

Sr and Nd isotopic compositions were measured by TIMS (Brussels University and Royal Museum for Central Africa, Belgium) on a VG sector 54 mass spectrometer. More details are provided in the Electronic Appendix A1.

The magmatic precursor of the 793-Ma-old metagabbros tapped a mantle source characterised by highly positive ε_{Nd} (+5.4 to +6.2) with low $^{87}\text{Sr}/^{86}\text{Sr}$ initial ratios (0.7027–0.7029), values that are close to depleted mantle composition at 793 Ma (ε_{Nd} : +6; $^{87}\text{Sr}/^{86}\text{Sr}$: 0.7023; Salters and Stracke 2004; Fig. 13). Nd T_{DM} model ages (818–960 Ma; calculated with depleted mantle evolution curve of Nelson and DePaolo 1984, only for samples having $^{147}\text{Sm}/^{144}\text{Nd} < 0.18$) are only slightly older than the magmatic crystallisation ages; this can be interpreted as the involvement of a limited quantity of an old radiogenic component in the mantle source of the metagabbros precursor. Pyroxenites (Fig. 13) have slightly lower ε_{Nd} (+4.9 to +5.6) with more radiogenic Sr isotopic composition ($^{87}\text{Sr}/^{86}\text{Sr}$: 0.7027–0.7034). The different rocks from the upper unit (quartz-gabbros, tonalites, hornblende-gabbros)

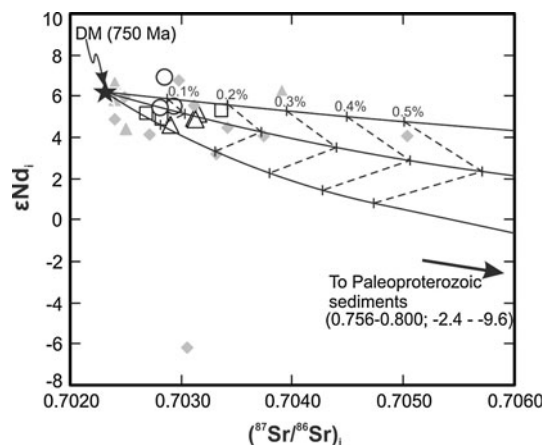


Fig. 13 Sr-Nd isotopic composition of Amalaoulaou rocks compared to composition of Tilemsi oceanic arc samples (grey triangles, Dostal et al. 1994) and the Kabyé continental arc (grey diamonds, Duclaux et al. 2006). Poles of the mixing hyperbolas are the depleted mantle of Salters and Stracke (2004) and Paleoproterozoic (meta-)sediments from the West African Craton (Roddaz et al. 2007). Same symbols as in Fig. 10

show lower ε_{Nd} (+4.6 to +5.2) and accordingly higher initial $^{87}\text{Sr}/^{86}\text{Sr}$ ratios (0.7028–0.7031) but are still close to the depleted mantle composition at 730 Ma.

Discussion

The Amalaoulaou complex is a Neoproterozoic intra-oceanic island arc

The intra-oceanic character of Amalaoulaou is demonstrated by several evidences. The absence of (meta-) sedimentary rocks and felsic orthogneiss contrasts with continental arcs located along the same Pan-African suture zone in the Adrar des Iforas (Fig. 1; Liégeois et al. 1987; Caby et al. 1989; Dostal et al. 1996) or to the south in Benin (Kabyé arc, Duclaux et al. 2006). On the other hand, Amalaoulaou correlates with the Tilemsi oceanic island arc to the north even if the latter is limited to the shallow sections of an island arc (Fig. 1; Caby et al. 1989). The metagabbros have similar geochemical fingerprint to the Jijal melt-like mafic rocks from the Kohistan oceanic arc and island arc tholeiites (IAT) from the Caribbean (Figs. 10, 11, 12), and quartz-gabbros are strikingly similar to rocks from the Tilemsi and Talkeetna oceanic arcs (Figs. 10, 11, 12). Lavas from continental arcs are by contrast dominated by calc-alkaline Si-rich primitive melts (andesitic basalt to andesite) and generally show higher K, Th and LREE contents as well as $(\text{La}/\text{Sm})_N$ ratios. Sr-Nd isotopic compositions of the Amalaoulaou arc are homogeneous and strongly depleted ($(^{87}\text{Sr}/^{86}\text{Sr})_i$: 0.7027–0.7034; ε_{Nd} : +4.5 to +6.0) and preclude a significant contamination of the

parental magmas by continental crust material. These narrow ranges of isotopic compositions (Fig. 13) are indeed characteristic of lavas and cumulates forming modern and Neoproterozoic intra-oceanic arcs (Izu-Bonin-Marianna system: 0.7026–0.7043; ε_{Nd} : +4 to +9; Stern et al. 2003; Tilemsi Neoproterozoic island arc: $(^{87}\text{Sr}/^{86}\text{Sr})_{730 \text{ Ma}}$: 0.7024–0.7039; ε_{Nd} : +4.4–6.6; Caby et al. 1989) and not of continental arc rocks (Andean arc: $^{87}\text{Sr}/^{86}\text{Sr}$: 0.704–0.7187; ε_{Nd} : −10.2 to +4.9; data from the GEOROC online database; Neoproterozoic continental Kabyé arc: $^{87}\text{Sr}/^{86}\text{Sr}$: 0.7015–0.7051, ε_{Nd} : −6.6 to +9.4; Duclaux et al. 2006).

Building of the root and middle crust of the Amalaoulaou intra-oceanic arc

The deep and medium sections of the Amalaoulaou arc have been built during two main magmatic inputs (stages 1 and 2) with contrasted geochemical characteristics and level of emplacement. A late-magmatic event is represented by low volume of tonalite pegmatite emplaced around 660 Ma but will not be discussed furthermore.

Magmatic stage 1

The magmatic precursors of metagabbros have been emplaced at oceanic upper mantle depth corresponding to a pressure of about 9.5 ± 1.5 kbar, probably around 800 Ma. Metagabbros have a melt-like geochemical signature; their parental melt (Mg#: 49–63) shows characteristic island arc tholeiite (IAT) fingerprints, i.e. high FeO/MgO ratios and low SiO_2 , depletion in LREE, low-amplitude negative Nb anomalies (Fig. 12a) and Sr-Nd isotopic composition close to depleted mantle (DM) values at 800 Ma (Fig. 13). The low La/Sm chondrite-normalised ratios (<1) argue for the involvement of a depleted mantle source, and the higher

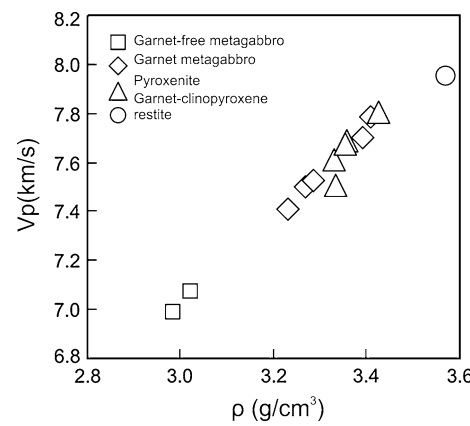


Fig. 14 Density versus P-wave velocity for Amalaoulaou lower crustal rocks. V_p and ρ have been computed with the macro of Hacker and Abers (2004) with the modal proportions and mineral compositions presented in this paper

Th/Nb (0.05–0.16) compared to N-MORB values (<0.07) show that melts or fluids from recycled sediments have been mixed with this depleted mantle source (Plank 2005) to form the metagabbros precursor. Semiquantitative modelling of Sr–Nd isotopic composition (Fig. 14) using a mixing hyperbola between the DM (Salters and Stracke 2004) and Proterozoic sediments from the West African craton (Roddaz et al. 2007) shows that less than 0.1% of a sedimentary component has to be added to the depleted mantle source to reproduce the isotopic composition of the metagabbros. Mafic rocks with very similar geochemical signatures characterise the immature stage of the Kohistan arc (Jijal complex, Dhuime et al. 2007; Figs. 11a and 12a) and of the Greater Antilles arc (Marchesi et al. 2007).

Magmatic stage 2

The 730-Ma-old quartz-gabbros, tonalites and hornblende-gabbros have been emplaced in the middle arc crust (5 ± 0.5 kbar). Despite variations in major element composition, they show similar trace element distribution. They are tholeiitic, melt-like rocks, primitive or differentiated (SiO_2 : 46–66; Mg#: 37–67) but with higher $(\text{La}/\text{Sm})_N$ ratios (>1; Fig. 11c) compared to metagabbros and more pronounced Nb-Ta negative anomalies (Fig. 12c). Accordingly, the Th/Nb ratios are higher (0.06–0.17) when compared to the metagabbro; it indicates a higher proportion of sedimentary components in the mantle source of the parental melts. Sr–Nd isotopic compositions point to a sediment proportion between 0.1 and 0.2% in the mantle wedge at 730 Ma (Fig. 13). These melts are comparable to mafic and felsic plutonic rocks emplaced in the middle and upper crust of the Talkeetna island arc (Greene et al. 2006). They likely reflect a more mature stage in the evolution of the Amalaoulaou arc.

An evolution of the composition of mantle source and parental melts with time is usual in island arcs. It can result from the modification of the partial melting regime and of the amount and nature of recycled sedimentary material (fluid or melt) delivered by the subducting slab (Dhuime et al. 2007; Reagan et al. 2008; Straub et al. 2010).

Maturation of the arc root

The metagabbro unit was affected by a metamorphic event leading to dehydration and partial melting of the arc root (Berger et al. 2009). Garnet pyroxenites and garnet metagabbros record higher T and/or P of equilibration (up to 900°C at $P \geq 10$ kbar) compared to spinel pyroxenites and garnet-free metagabbros (700–750°C at 7–8 kbar). This event is tentatively interpreted as the maturation stage of the oceanic arc (Berger et al. 2009) similarly to the interpretation of the Kohistan arc root (Burg et al. 1998; Garrido et al. 2006). It corresponds to the burial of the arc root to HT-HP

conditions with localised dehydration and dehydration-melting thanks to high magmatic input in the upper and middle arc crust. The maturation stage has not modified the bulk composition of the arc root, but it has a strong impact on the physical properties of the lowermost crust (see below).

Comparison with the deep section of Mesozoic arcs and implications for the crust-mantle transition under arcs

The Cryogenian Amalaoulaou intra-oceanic arc shares many similarities with the Jurassic Kohistan arc in the Himalayan belt and the Talkeetna arc section in Alaska. Primary magmas emplaced in the Amalaoulaou arc root have the same trace element signature as the Jijal melt-like mafic rocks (Dhuime et al. 2007; Figs. 11a and 12a). In addition, plutonic rocks emplaced in the middle arc crust are closely comparable to the lithologies forming the middle crust of the Talkeetna arc (Greene et al. 2006; Figs. 11c and 12c). These observations show that the processes of melt formation under intra-oceanic arcs have not significantly changed between the Neoproterozoic and the Mesozoic eras. Berger et al. (2009) already pointed out that crustal thickening at Amalaoulaou has strongly modified the structure and physical properties of the arc root by generating dense garnet-bearing lithologies in response to dehydration and dehydration–melting reactions. The same processes have been proposed for the evolution of the Jijal complex forming the base of the Kohistan arc (Yamamoto and Yoshino 1998; Yoshino and Okudaira 2004).

The existence of exposed deep arc sections is an excellent opportunity for comparing information brought by geophysical methods on the structure and composition of the crust-to-mantle transition zone under oceanic arcs. The deepest part of the Amalaoulaou arc is mainly composed of former gabbros now transformed into amphibolised garnet-bearing and garnet-free granulites. Densities and seismic wave velocities (V_p) of the main rock types (Fig. 14, Table 1) forming the base of the Amalaoulaou arc have been computed with the algorithm of Hacker and Abers (2004). Following their method, we have used the mineral composition measured by microprobe and the modal proportions measured on thin section. However, because the original composition of plagioclase is not known and because secondary brown amphibole has grown at the expense of clinopyroxene in most samples, the results are quite imprecise, but they give an idea of the physical properties of the lowermost arc crust. We adopted a conservative An_{80} value, a typical plagioclase composition in lower crustal garnet-bearing and garnet-free gabbros from island arcs (DeBari and Coleman 1989), also in agreement with the dominant epidote as secondary phase. The proportion of clinopyroxene in the granulitic precursor was computed as

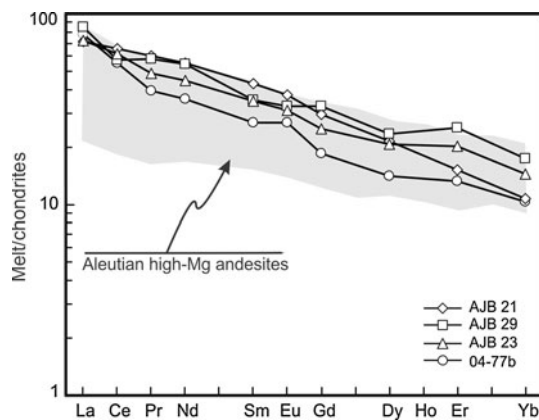


Fig. 15 REE pattern of the parental melt of the pyroxenite dykes. Comparison data are from the online GEOROC database

the sum of clinopyroxene and amphibole proportions. Granulites devoid of garnet have rather low densities, around 3 g/cm^3 and accordingly V_p in the range of lower crustal basic rocks (7–7.1 km/s). In garnet-bearing samples, the computed density strongly depends on the proportion of garnet: it varies from 3.2 to 3.3 for rocks with 20 vol.% garnet to 3.4–3.6 for rocks with 30–40% garnet, the highest density being reached in the restitic garnet-clinopyroxene-rutile sample. V_p values for these samples (7.7–7.9 km/s) can be as high as upper mantle values under modern mature island arcs (7.7–8.0 km/s; Takahashi et al. 2008). Pyroxenites have also high densities (3.3–3.4, V_p : 7.6 km/s) with the highest value for garnet pyroxenites (3.4, V_p : 7.8 km/s). The presence of dispersed dense lithologies towards the base of the arc crust explain why in many active island arcs the seismic wave velocities increase progressively from lower crust to upper mantle (Takahashi et al. 2008) and why the lower crust has high V_p (up to 7.4 km/s) above an upper mantle with relatively low V_p (7.6–8.0 km/s). Indeed, this transition zone may be structured as a dense garnet-granulites and pyroxenites in the lowermost crust, underlain by an upper mantle containing pyroxenites (formed by melt-rock interactions or delaminated) and garnet-granulites (former intrusions of gabbros) similarly as exposed in the Kohistan arc root (Burg et al. 1998). However, all these dense pyroxene- and garnet-bearing rocks are present only in small proportions in the lowermost Amalaoulaou root: pyroxenites are limited to few dykes and garnet-rich samples are restricted to former zones of fluid and/or melt circulation and zones where the gabbros partially melted.

The origin of pyroxenites in the Amalaoulaou intra-oceanic arc

Previous work has shown that garnet-rutile clinopyroxenite lenses are residues formed by dehydration melting of

metagabbros during crustal thickening of the Amalaoulaou arc (Berger et al. 2009). The plagioclase, the spinel and the garnet pyroxenites are cropping out as dykes cutting across the metagabbros; they can consequently be interpreted as magmatic bodies. The high Mg# (88–92, Fe as total iron) of clinopyroxene cores (i.e. not affected by metamorphic garnet growth) in spinel pyroxenites indicates that the Mg# of parental melt was between 67 and 78, considering a Fe–Mg K_d in the range 0.27–0.31 (Müntener et al. 2001). Such melt is significantly more magnesian than the IAT-melt represented by the metagabbros precursor (Mg#: 49–63). In the spinel pyroxenites, the phase that dominantly hosts REEs is the clinopyroxene because REE partition preferentially into this phase rather than in orthopyroxene and in spinel. The REE content of the clinopyroxene parental melt has been computed using the cpx/melt partition coefficients of Hart and Dunn (1993), after correction of the bulk-rock REE content for the dilution effect generated by the presence of orthopyroxene and spinel. The calculated parental melt (Fig. 15) is REE-rich (10–100 times the chondritic values) with a steep LREE-enriched pattern (La/Yb_N : 4.8–5). No comparable melt has been found at Amalaoulaou; however, high-Mg# and high REE island arc magma strongly enriched in LREE is characteristic of high-Mg# andesites ($\text{Mg#} > 45$, up to 74; La/Yb_N : 2–6; 99 samples from the Aleutian arc in the online GEOROC database). A boninite melt (Mg# : 40–87) as parental magma is unlikely because most boninites have a flat or enriched HREE distribution compared to MREE, with low La/Yb_N ratios (most samples with $\text{La/Yb}_N < 2$; 199 data from the online GEOROC database). The source of Amalaoulaou pyroxenites is comparatively enriched (higher Sr isotope ratio and lower Nd isotopic ratio), confirming that the parental melt has been formed by processes different than those forming the magmatic precursor of metagabbros (close to IAT).

An origin of the pyroxenites by interaction between peridotite and a basaltic melt in magma conduits has been proposed for the pyroxenites of Kohistan (Garrido et al. 2007; Bouilhol et al. 2009), but it cannot be transposed to the Amalaoulaou arc where most pyroxenites form bodies cutting across older metagabbros. The mineral-like signature of pyroxenites, the more radiogenic isotopic ratios and their probable high-Mg andesitic parental melt can be explained by a combination of two processes. (1) Formation of high-Mg primitive andesites requires melting of a strongly metasomatised mantle source (Wood and Turner 2009 and references therein) with further possible melt-rock interactions during ascent in the mantle wedge (Kelemen 1995). The source of the pyroxenite parental melt was consequently enriched in incompatible elements including LREE; the enriched Sr–Nd isotopic signature of pyroxenites compared to metagabbros implies that significant proportions of an old radiogenic component is present

in the mantle source. These constraints could be met by a subduction component corresponding to older WAC-derived sediments, sediment partial melts or fluids (Fig. 13). High-Mg# andesites are common in modern island arcs (Kelemen et al. 2003), and consequently, they are likely to have been produced during the building of the Amalaoulaou arc. (2) Segregation of clinopyroxene in former melt conduits (dykes), probably by flowage differentiation in response to the Bagnold effect (Nkono et al. 2006). This is required by the mineral-like fingerprint of pyroxenites and their style of emplacement; the high Sr content of plagioclase pyroxenites and the slight positive Eu anomaly in sample 04–77 probably reflect limited segregation of plagioclase in the melt conduit.

Implications for the growth of the continental crust

Island arcs are expected to be the fundamental bricks of continental crust (Taylor and McLennan 1985; Stern 2010), but a major problem of this assumption is that continental crust has a bulk andesitic composition while island arcs are formed by progressive inputs of basaltic magmas with minor primitive high-Mg# andesites and boninites (Kelemen et al. 2003; Garrido et al. 2006; Stern 2010 and references therein). A fundamental question is to know whether this andesitic composition can be reached by delamination of ultramafic cumulates and restites or whether primitive melts forming ancient island arcs are more evolved than modern arcs. The lower and middle crusts of the Amalaoulaou arc have a basaltic bulk composition (Fig. 10), but the metagabbros have low Mg# (49–63) are iron-rich when compared to primitive magmas from modern island arcs (average Mg#: 65–71; Kelemen et al. 2003, Fig. 10). The low Cr and Ni contents of melt-like metagabbros (120–200 ppm and 24–65 ppm, respectively) compared to primitive island arc lavas (350–1,000 ppm and 130–440 ppm, respectively; Fig. 10) probably show that ferromagnesian phases (olivine, pyroxene and spinel) have been fractionated but ultramafic cumulates are lacking at Amalaoulaou. A simple mass balance calculation demonstrates that when 10–20 vol.% of ultramafic cumulate is added to the mean composition of melt-like metagabbros, the resulting magma has a Mg# comparable to mean primitive Mariana arc lavas (65; Kelemen et al. 2003). The lack or paucity of primitive high-Mg cumulates is also a characteristic of the Mesozoic oceanic arcs, namely the Talkeetna section and the Kohistan complex (Greene et al. 2006; Garrido et al. 2007). This has been explained either by the more Fe-rich and Si-rich nature of primitive melts compared to modern arcs or by the delamination of dense primitive cumulates (mainly pyroxenites) forming the base of the arc root. Our preferred hypothesis for the Amalaoulaou arc is that ultramafic cumulates have been formed

but are lacking in the present day structure of the arc complex, probably as a consequence of delamination of the lowermost arc crust.

Intra-oceanic arcs, such as Amalaoulaou, Kohistan and Talkeetna, can consequently not be taken as unique examples of fundamental bricks forming the continental crust because even if delamination of ultramafic cumulates and/or residues occurred, they are all of basaltic bulk composition. Archean oceanic arcs, instead, are expected to be more felsic because subduction of mafic crust would induce partial melting of the latter and the production of tonalite-trondhjemite-granodiorite melts (Drummond and Defant 1990) forming batholiths intruding the supra-subduction oceanic crust with dense garnet-clinopyroxene residues sinking into the mantle. A model combining Archean-like rapid crustal growth involving the accretion of bimodal basaltic-felsic arcs with the addition of basaltic island arcs since the Late-Proterozoic can be envisaged to explain the andesitic composition of the bulk continental crust.

Geodynamical implications

Age of the metamorphic events

Due to the lack of direct dating of the various events of metamorphism and deformation, only relative ages can be provided.

- Metamorphic phase 1 is a granulitic/melting event that occurred at 900–1,000°C and 10–12 kbar (stages C and D on Fig. 9). At Amalaoulaou, the role of magma intrusion in the generation of the granulite-facies overprint is locally evidenced by the development of garnet within the metagabbros at the contact zone with pyroxenite and felsic dykes (Berger et al. 2009). This metamorphism is thus bracketed between c. 793 Ma (age of the protoliths) and c. 701 Ma (the rocks of this age are not affected).
- Metamorphic phase 2 is a high-temperature shearing (725–875°C, 8–11 kbar; stage E on Fig. 9), leading to the transformation of garnet-granulites into protomylonitic metagabbros with brown pargasite. It affected these rocks during the final stages of the granulitic-melting event (phase 1). Indeed, garnet-bearing leucocratic veins (emplaced at $P > 10$ kbar) are affected by this deformation event whereas garnet-absent veins ($P < 10$ kbar) are undeformed by this HT shearing (Fig. 5a, b). This event is thus related to partial exhumation of the arc root. Many structural and metamorphic similarities with the Kohistan arc root (Arbaret and Burg 2003, Burg et al. 2006) suggest that it is linked to rifting or detachment fault within the arc.

As phase 1, this second phase is bracketed between c. 793 Ma and c. 701 Ma.

- Metamorphic phase 3 is a low-temperature amphibolite-facies event (stage F on Fig. 9), recorded in the epidote–amphibolite unit and affecting only the metagabbro unit. It has affected only the metagabbros. The peculiar P-T conditions associated with this event ($\sim 550^{\circ}\text{C}$, 6–9 kbar) are closely similar to the retrograde exhumation path of the Gourma continental UHP eclogites (Caby et al. 1989; Caby 2003). It can thus be interpreted as a late exhumation phase of the Amalaoulaou arc.
- Metamorphic phase 4 occurred under greenschist facies conditions and is most probably responsible for the youngest LT-LP shear zone and recrystallisation observed in the whole Amalaoulaou complex. It can be reasonably related with the nappe stacking (Caby 1979, 2003) that occurred during the continental collision with the main part of the Tuareg shield between 620 and 580 Ma (Liégeois et al. 1987; Attoh et al. 1997).

Regional constraints

To the north of Amalaoulaou, the Tilemsi oceanic arc can be considered as the upper crust superstructure equivalent of the Amalaoulaou complex. Considering the available geochronological data, the Tilemsi arc was active prior to 726 Ma (age of oceanic metadiorites cutting across volcano-sedimentary successions emplaced in an oceanic arc setting) and at 710 Ma, corresponding to the emplacement of a plagiogranitic mobilisate (Caby et al. 1989). The Tilemsi island arc superstructure is thus subcontemporaneous with Amalaoulaou magmatic stage 2. If relics of island arcs are preserved along the eastern Pan-African WAC suture, there is only a few evidences for the presence of fore-arcs and back-arcs, except in the Anti-Atlas belt of Morocco where probable fore-arc, arc and back-arc systems are identified (Thomas et al. 2004). In Mali, two occurrences of mafic–ultramafic associations are known: (1) the Timetrine serpentinites and (meta) basalts, with locally preserved pillow structures and (2) a few serpentinite outcrops in the Northern part of the Gourma belt (Fig. 3). However, no detailed investigations have been performed on these rocks, and their tectonic setting cannot be further precised.

To the east of the Tilemsi-Amalaoulaou oceanic terranes are located the continental active margin terranes of the Adrar des Iforas (Fig. 1). In the Kidal terrane (Black et al. 1994), an early stage of ocean-continent subduction, represented by few gneissic tonalitic plutons, has been dated at 696 ± 5 Ma (Caby and Andréopoulos-Renaud 1985) and 716 ± 6 Ma (Bruguier et al. 2008). They are covered by

active margin-type volcano-sedimentary sequence, one of them being dated at 630 ± 13 Ma (Liégeois 1988) accompanied by tonalitic and granodioritic plutons of the same age (635 ± 5 Ma; Caby et al. 1989; 634 ± 8 Ma; Bruguier et al. 2008). They are followed by the huge composite Iforas batholith that intruded between 620 and 580 Ma in a post-collisional setting through transpressive movements (Liégeois et al. 1987; Liégeois 1988; Liégeois et al. 1998). This indicates that (1) a subduction period occurred below the Adrar des Iforas active margin at least between 716 and 630 Ma; (2) two subductions coexisted at least between 716 and 660 Ma, an intra-oceanic subduction represented by the Amalaoulaou arc and an ocean-continent subduction below the Iforas active margin; (3) this active margin collided with the WAC between 630 and 620 Ma, which corresponds to the UHP metamorphism in Gourma (623 ± 3 Ma; Jahn et al. 2001).

Geodynamical evolution of the Amalaoulaou arc

The magmatic activity in the Amalaoulaou intra-oceanic island arc started at c. 790 Ma, with the emplacement of LREE-depleted tholeitic mafic melts (nascent or immature stage). The maturation of the arc is evidenced by the emplacement of melts tapped from a mantle source enriched in recycled sedimentary material and by the HT-HP granulitic phase in the root. This is followed by a partial exhumation of the arc root (metamorphic phase 2 associated with shearing) due to intra-oceanic rifting or maybe to the proximity of the WAC. This phase is followed at c. 700 Ma by the magmatic phase 2 represented by slightly LREE-enriched tholeiitic mafic to felsic rocks.

The LT amphibolite event (metamorphic phase 3) is linked to the accretion of the Amalaoulaou island arc towards the WAC, either at (1) 700–660 Ma and a second time during the exhumation of the Gourma continental UHP eclogites at c. 623 Ma or (2) only in one stage at c. 623 Ma, the absence of magmatic activity in the 660–623 Ma period being attributed to the WAC continental subduction. Finally, the metamorphic phase 4 corresponds to the nappe stacking under greenschist facies conditions during the major transpressive period (620–580 Ma).

The oceanic evolution of the Amalaoulaou island arc and its final accretion towards the West African craton fit within the general Pan-African cycle ending with the Gondwana amalgamation, especially in its Saharan part. In the Tuareg shield, the period between 850 and 640 Ma is mainly represented by juvenile lithologies that developed within the Pharusian Ocean and that successively accreted towards either the West African craton (Caby et al. 1982; Liégeois et al. 1987; this study), the LATEA metacraton

(Caby and Andreopoulos-Renaud 1987; Liégeois et al. 2003) or the Saharan metacraton (Liégeois et al. 1994; Henry et al. 2009). The final closure of the different branches of the Pharusian Ocean occurred during the continental collision between the West African craton, the LATEA and Saharan metacratons during the 630–580 Ma period (Black et al. 1994; Liégeois et al. 1987; 2003; Jahn et al. 2001; Caby 2003), corresponding to the western Gondwana supercontinent amalgamation. The story that occurred on the eastern side of the Sahara is similar. There also the 850–630 Ma period is marked by the opening and the closing of the wide Mozambique Ocean and the generation of the huge juvenile Arabo-Nubian Shield including more easterly terranes (Sato et al. 2011) mostly by island arcs accretion (see Stern and Johnson 2010). The main closure of the Mozambique Ocean corresponds to the eastern Gondwana amalgamation marked by the East African orogen and occurred within the 630–580 Ma time interval (Stern 1994; Küster et al. 2008; Stern and Johnson 2010), with late events that reached early Cambrian (Stern 1994; Sato et al. 2011) leading to the formation of Greater Gondwana.

Conclusions

The Amalaoulaou complex represents the exposed section of a Neoproterozoic intra-oceanic arc from the root to the medium crust. The successive magmatic inputs reflect a progressive change of mantle source composition with a dominant depleted mantle component for 793-Ma-old metagabbros (nascent stage) and a more significant, although still minor (0.2%), involvement of recycled sediments in the source of younger gabbros (~701 Ma, mature stage) with late minor magmatic activity around 660 Ma. The oldest metamorphic event (phase 1) recorded in the arc root induced dehydration and localised melting in response to arc thickening (maturation of the arc). HT shearing (metamorphic phase 2) affecting the metagabbros slightly after the granulitic event is tentatively linked to partial exhumation of the arc root accommodated by detachment faults or partial rifting of the body. The accretion of the Amalaoulaou arc onto the WAC passive margin is evidenced by two phases of metamorphism (phases 3 and 4), but the exact timing and significance of these events are not well constrained.

The lowermost crust of the Amalaoulaou arc root is mainly composed of metagabbros having melt-like geochemical fingerprints with a few pyroxenites of cumulates origin. Dense rocks (3.3–3.6) are either partial melting/dehydration residues dominated by garnet-clinopyroxene assemblages or pyroxene segregates representing the former magma path of high-Mg andesites. However, the dense

rocks form a low volumetric proportion and are dispersed in the arc root; this precludes massive delamination of the deep crustal section during or after the maturation stage. Parental magmas at Amalaoulaou have already crystallised ultramafic cumulates before being emplaced in the lower and middle crust, but these cumulates are missing. The bulk composition of the exposed section is however still basaltic, and the probable delamination of these ultramafic cumulates did not induce a compositional change from basaltic to andesitic, i.e., close to the bulk continental crust.

Compared to other well-studied and more recent exhumed section of oceanic arcs, the Amalaoulaou complex shares same geochemical fingerprints and metamorphic evolution. It can consequently be concluded that processes responsible for building and differentiation of Neoproterozoic oceanic arcs are similar to those forming younger recent arcs. If we consider that accretion of island arcs is the main mechanism of continental growth, those formed since the Late Precambrian cannot be the fundamental bricks of the andesitic continental crust because they have a basaltic bulk composition. A transition from the accretion of intermediate to felsic Archean-like island arcs to basaltic island arcs since the Late-Proterozoic is then required to match the andesitic composition of continental crust.

Acknowledgments JB and RC want to thank all the participants to the IGCP 485 meeting in Gao for fruitful discussions. B. Dhuime and D. Bosch are acknowledged for providing some key Amalaoulaou samples that were integrated in this study. Discussions with JP Burg and JL Bodinier about Kohistan arc pyroxenites were helpful. Comments of the three reviewers (C. Garrido, R. Stern and J-P. Burg) have significantly improved the organisation and the quality of the paper. J. Touret is also acknowledged for its editorial work.

References

- Andersen DJ, Lindsley DH, Davidson PM (1993) Quilf - a pascal program to assess equilibria among Fe-Mg-Mn-Ti oxides, pyroxenes, olivine, and quartz. Comput Geosci 19:1333–1350
- Anderson DL (2005) Large igneous provinces, delamination, and fertile mantle. Elements 1:271–275
- Arbaret L, Burg JP (2003) Complex flow in lowest crustal, anastomosing mylonites: strain gradients in a Kohistan gabbro, northern Pakistan. J Geophys Res 108:2467
- Attoh K, Dallmeyer RD, Affaton P (1997) Chronology of nappe assembly in the Pan-African Dahomeyide orogen, West Africa: evidence from Ar-40/Ar-39 mineral ages. Prec Res 82:153–171
- Bayer R, Lesquer A (1978) Les anomalies gravimétriques de la bordure orientale du craton ouest africain; géométrie d'une suture pan-africaine. Bull Soc Géol Fr 20:863–876
- Behn MD, Kelemen PB (2006) Stability of arc lower crust: Insights from the Talkeetna arc section, south central Alaska, and the seismic structure of modern arcs. J Geophys Res Solid Earth 111:B11207
- Berger J, Caby R, Liégeois JP, Mercier JCC, Demaiffe D (2009) Dehydration, melting and related garnet growth in the deep root of the Amalaoulaou Neoproterozoic magmatic arc (Gourma, NE Mali). Geol Mag 146:173–186

- Black R, Latouche L, Liégeois JP, Caby R, Bertrand JM (1994) Pan-African displaced terranes in the Tuareg Shield (Central Sahara). *Geology* 22:641–644
- Bouilhol P, Burg JP, Bodinier JL, Schmidt MW, Dawood H, Hussain S (2009) Magma and fluid percolation in arc to forearc mantle: evidence from Sapat (Kohistan, Northern Pakistan). *Lithos* 107:17–37
- Bruguier O, Bosch D, Caby R, Galland B, Hammor D (2008) Sampling an active continental paleo-margin: a LA-ICP-MS U-Pb zircon study from the Adrar des Iforas (Mali). *Geochim Cosmochim Acta* 72:A118
- Burg JP, Bodinier JL, Chaudhry S, Hussain S, Dawood H (1998) Infra-arc mantle-crust transition and intra-arc mantle diapirs in the Kohistan complex (Pakistani Himalaya): petro-structural evidence. *Terra Nova* 10:74–80
- Burg JP, Jagoutz O, Dawood H, Hussain SS (2006) Precollision tilt of crustal blocks in rifted island arcs: structural evidence from the Kohistan Arc. *Tectonics* 25:TC5005
- Buscail F, Caby R (2005) Notice explicative et carte géologique du Gourma oriental au 1/200 000 Ansongo-Amalaoulaou. Direction Nationale des Mines et de la Géologie, Bamako, Mali
- Caby R (1979) Les nappes précambriniennes du Gourma dans la chaîne pan-africaine du Mali. *Rev Géol Dyn Géog Phys* 21:367–376
- Caby R (1994) Precambrian coesite from Northern Mali—1st record and implications for plate-tectonics in the trans-saharan segment of the Pan-African belt. *Eur J Min* 6:235–244
- Caby R (2003) Terrane assembly and geodynamic evolution of central-western Hoggar: a synthesis. *J Afr Earth Sci* 37:133–159
- Caby R, Andreopoulos-Renaud U (1987) Le Hoggar oriental, bloc cratonisé à 730 Ma dans la chaîne pan-africaine du Nord du continent africain. *Precambrian Res* 36:335–344
- Caby R, Andréopoulos-Renaud U (1985) Etude pétrostructurale et géochronologie U/Pb sur zircon d'une métadiorite quartzique de la chaîne pan-africaine de l'Adrar des Iforas (Mali). *Bull Soc Géol Fr* 1:899–903
- Caby R, Andreopoulos-Renaud U, Gravelle M (1982) Cadre géologique et géochronologie U/Pb sur zircon des batholithes précoces dans le segment panafricain du Hoggar central (Algérie). *Bull Soc Géol Fr* 7:876–882
- Caby R, Andréopoulos-Renaud U, Pin C (1989) Late Proterozoic arc-continent and continent-continent collision in the Pan-African Trans-Saharan Belt of Mali. *Can J Earth Sci* 26:1136–1146
- Caby R, Buscail F, Dembele D, Diakite S, Sacko S, Bal M (2008) Neoproterozoic garnet-glaucophanites and eclogites: new insights for subduction metamorphism of the Gourma fold and thrust belt (eastern Mali). *Geol Soc Lond Spec Pub* 297:203–216
- de la Boisse H (1979) Pétrologie et géochronologie des roches cristallophylliennes du bassin de Gourma (Mali), conséquences pétrogénétiques. Unpublished PhD thesis, Montpellier, p 54
- de la Boisse H (1981) Sur le métamorphisme du micaschiste éclogitique de Takamba (Mali) et ses conséquences paléogéodynamiques au Précambrien supérieur. *C R Soc Géol Fr* 3:97–100
- Debari SM, Coleman RG (1989) Examination of the deep levels of an island-arc—evidence from the Tonsina ultramafic-mafic assemblage, Tonsina, Alaska. *J Geophys Res Solid Earth Planets* 94:4373–4391
- Dhuime B, Bosch D, Bodinier JL, Garrido CJ, Bruguier O, Hussain SS, Dawood H (2007) Multistage evolution of the Jijal ultramafic-mafic complex (Kohistan, N Pakistan): implications for building the roots of island arcs. *Earth Planet Sci Lett* 261:179–200
- Dhuime B, Bosch D, Garrido CJ, Bodinier JL, Bruguier O, Hussain SS, Dawood H (2009) Geochemical architecture of the lower- to middle-crustal section of a paleo-island arc (Kohistan complex, Jijal/Kamila area, Northern Pakistan): implications for the evolution of an oceanic subduction zone. *J Petrol* 50:531–569
- Dostal J, Dupuy C, Caby R (1994) Geochemistry of the neoproterozoic tilemsi belt of Iforas (Mali, Sahara)—a crustal section of an oceanic island-arc. *Precambrian Res* 65:55–69
- Dostal J, Caby R, Dupuy C, Mevel C, Owen JV (1996) Inception and demise of a Neoproterozoic ocean basin: evidence from the Ougda complex, western Hoggar (Algeria). *Int J Earth Sci* 85:619–631
- Drummond MS, Defant MJ (1990) A model for Trondhjemite-tonalite-dacite genesis and crustal growth via slab melting: archean to modern comparisons. *J Geophys Res* 95:21503–21521
- Duclaux G, Menot RP, Guillot S, Agbossoumonde Y, Hilairet N (2006) The mafic layered complex of the Kabyé massif (north Togo and north Benin): evidence of a Pan-African granulitic continental arc root. *Prec Res* 151:101–118
- Féménias O, Mercier JCC, Nkono C, Diot H, Berza T, Tatu M, Demaiffe D (2006) Calcic amphibole growth and compositions in calc-alkaline magmas: evidence from the Motru Dike Swarm (Southern Carpathians, Romania). *Am Min* 91:73–81
- Fitzsimons ICW, Harley SL (1994) The influence of retrograde cation-exchange on granulite P-T estimates and a convergence technique for the recovery of peak metamorphic conditions. *J Petrol* 35:543–576
- Ganguly J (1979) Garnet and clinopyroxene solid solutions, and geothermometry based on Fe-Mg distribution coefficient. *Geochim Cosmochim Acta* 43:1021–1029
- Garrido CJ, Bodinier JL, Burg JP, Zeilinger G, Hussain SS, Dawood H, Chaudhry MN, Gervilla F (2006) Petrogenesis of mafic garnet granulite in the lower crust of the Kohistan paleo-arc complex (Northern Pakistan): implications for intra-crustal differentiation of island arcs and generation of continental crust. *J Petrol* 47:1873–1914
- Garrido CJ, Bodinier JL, Dhuime B, Bosch D, Chanefo I, Bruguier O, Hussain SS, Dawood H, Burg JP (2007) Origin of the island arc Moho transition zone via melt-rock reaction and its implications for intracrustal differentiation of island arcs: evidence from the Jijal complex (Kohistan complex, northern Pakistan). *Geology* 35:683–686
- Greene AR, DeBari SM, Kelemen PB, Blusztajn J, Clift PD (2006) A detailed geochemical study of island arc crust: the Talkeetna Arc section, south-central Alaska. *J Petrol* 47:1051–1093
- Hacker BR, Abers GA (2004) Subduction factory 3: an excel worksheet and macro for calculating the densities, seismic wave speeds, and H₂O contents of minerals and rocks at pressure and temperature. *Geochem Geophys Geosyst* 5
- Harley SL (1984a) An experimental study of the partitioning of Fe and Mg between garnet and orthopyroxene. *Contrib Miner Petrol* 86:359–373
- Harley SL (1984b) The solubility of alumina in orthopyroxene coexisting with garnet in FeO-MgO-Al₂O₃-SiO₂ and CaO-FeO-MgO-Al₂O₃-SiO₂. *J Petrol* 25:665–696
- Hart SR, Dunn T (1993) Experimental cpx/melt partitioning of 24 trace-elements. *Contrib Miner Petrol* 113:1–8
- Henry B, Liegeois JP, Nouar O, Derder MEM, Bayou B, Bruguier O, Ouabadi A, Belhai D, Amenna M, Hemmi A, Ayache M (2009) Repeated granitoid intrusions during the Neoproterozoic along the western boundary of the Saharan metacraton, Eastern Hoggar, Tuareg shield, Algeria: an AMS and U-Pb zircon age study. *Tectonophysics* 474:417–434
- Hofmann AW (1988) Chemical differentiation of the earth—the relationship between mantle, continental-crust, and oceanic-crust. *Earth Planet Sci Lett* 90:297–314
- Holbrook WS, Lizarralde D, McGeary S, Bangs N, Diebold J (1999) Structure and composition of the Aleutian island arc and implications for continental crustal growth. *Geology* 27:31–34
- Jahn B, Caby R, Monie P (2001) The oldest UHP eclogites of the world: age of UHP metamorphism, nature of protoliths and tectonic implications. *Chem Geol* 178:143–158

- Jan M, Howie RA (1981) The mineralogy and geochemistry of the metamorphosed basic and ultrabasic rocks of the Jijl complex, Kohistan, NW Pakistan. *J Petrol* 22:85–126
- Jull M, Kelemen PB (2001) On the conditions for lower crustal convective instability. *J Geophys Res Solid Earth* 106:6423–6446
- Kay RW, Kay SM (1988) Crustal recycling and the Aleutian arc. *Geochim Cosmochim Acta* 52:1351–1359
- Kelemen PB (1995) Genesis of high Mg-number andesites and the continental-crust. *Contrib Miner Petrol* 120:1–19
- Kelemen PB, Hanghøj K, Greene AR (2003) One view of the geochemistry of subduction-related magmatic arcs, with an emphasis on primitive andesite and lower crust. In: Heinrich DH, Karl KT (eds) *Treatise on geochemistry, the crust*, vol 3. Pergamon, Oxford, pp 593–659
- Küster D, Liégeois JP, Matukov D, Sergeev S, Lucassen F (2008) Zircon geochronology and Sr, Nd, Pb isotope geochemistry of granitoids from Bayuda Desert and Sabaloka (Sudan): evidence for a Bayudian event (920–900 Ma) preceding the Pan-African orogenic cycle (860–590 Ma) at the eastern boundary of the Saharan Metacraton. *Precambrian Res* 164:16–39
- Liégeois JP (1988) Le batholite composite de l'Adrar des Iforas (Mali). Académie Royale des Sciences d'Outre-Mer. Classe Sci Nat et Med Mémoire 8°. *Sci Géol* 22(2): 231
- Liégeois JP, Bertrand JM, Black R (1987) The subduction- and collision-related Pan-African composite batholith of the Adrar des Iforas (Mali); a review. *Geol J* 22:185–211
- Liégeois JP, Black R, Navez J, Latouche L (1994) Early and late Pan-African orogenies in the Aïr assembly of terranes (Tuareg shield, Niger). *Precambrian Res* 67:59–88
- Liégeois JP, Navez J, Hertogen J, Black R (1998) Contrasting origin of post-collisional high-K calc-alkaline and shoshonitic versus alkaline and peralkaline granitoids. The use of sliding normalization. *Lithos* 45:1–28
- Liégeois JP, Latouche L, Boughrara M, Navez J, Guiraud M (2003) The LATEA metacraton (Central Hoggar, Tuareg shield, Algeria): behaviour of an old passive margin during the Pan-African orogeny. *J Afr Earth Sci* 37:161–190
- Liou JG, Maruyama S, Cho M (1985) Phase equilibria and mineral parageneses of metabasites in low-grade metamorphism. *Min Mag* 49:321–333
- Liu J, Ye K (2004) Transformation of garnet epidote amphibolite to eclogite, western Dabie Mountains, China. *J Metam Geol* 22:383–394
- Lopez S, Castro A (2001) Determination of the fluid-absent solidus and supersolidus phase relationships of MORB-derived amphibolites in the range 4–14 kbar. *Am Min* 86:1396–1403
- Ludwig KR (2003) Isoplot 3.00: a geochronological toolkit for Microsoft Excel, Berkeley Geochronology Center Special Publication, p 70
- Marchesi C, Garrido CJ, Bosch D, Proenza JA, Gervilla F, Monie P, Rodriguez-Vega A (2007) Geochemistry of Cretaceous magmatism in eastern Cuba: recycling of North American continental sediments and implications for subduction polarity in the Greater Antilles paleo-arc. *J Petrol* 48:1813–1840
- McDonough WF, Sun SS (1995) The composition of the earth. *Chem Geol* 120:223–253
- Ménot RP (1980) Les massifs basiques et ultrabasiques de la zone mobile Pan-Africaine au Ghana, Togo et Benin; état de la question. *Bull Soc Geol Fr* 22:297–303
- Miller DJ, Christensen NI (1994) Seismic signature and geochemistry of an island-arc—a multidisciplinary study of the Kohistan accreted terrane, Northern Pakistan. *J Geophys Res Solid Earth* 99:11623–11642
- Moore JC, Diebold J, Fisher MA, Sample J, Brocher T, Talwani M, Ewing J, Vonhuene R, Rowe C, Stone D, Stevens C, Sawyer D (1991) Edge deep seismic-reflection transect of the Eastern Aleutian arc-Trench layered lower crust reveals underplating and continental growth. *Geology* 19:420–424
- Müntener O, Kelemen PB, Grove TL (2001) The role of H₂O during crystallization of primitive arc magmas under uppermost mantle conditions and genesis of igneous pyroxenites: an experimental study. *Contrib Miner Petrol* 141:643–658
- Nelson BK, DePaolo DJ (1984) 1, 700-Myr greenstone volcanic successions in southwestern North America and isotopic evolution of Proterozoic mantle. *Nature* 312:143–146
- Nimis P, Ulmer P (1998) Clinopyroxene geobarometry of magmatic rocks part 1: an expanded structural geobarometer for anhydrous and hydrous, basic and ultrabasic systems. *Contrib Miner Petrol* 133:122–135
- Nkono C, Femenias O, Diot H, Berza T, Demaiffe D (2006) Flowage differentiation in an andesitic dyke of the Motru Dyke Swarm (Southern Carpathians, Romania) inferred from AMS, CSD and geochemistry. *J Volcanol Geothermal Res* 154:201–221
- Pattison DRM (2003) Petrogenetic significance of orthopyroxene-free garnet plus clinopyroxene plus plagioclase ± quartz-bearing metabasites with respect to the amphibolite and granulite facies. *J Metam Geol* 21:21–34
- Plank T (2005) Constraints from thorium/lanthanum on sediment recycling at subduction zones and the evolution of the continents. *J Petrol* 46:921–944
- Rapp RP, Watson EB (1995) Dehydration melting of metabasalt at 8–32-Kbar—implications for continental growth and crust-mantle recycling. *J Petrol* 36:891–931
- Reagan MK, Hanan BB, Heizler MT, Hartman BS, Hickey-Vargas R (2008) Petrogenesis of volcanic rocks from Saipan and Rota, Mariana Islands, and implications for the evolution of Nascent Island arcs. *J Petrol* 49:441–464
- Reichelt R (1972) Géologie du Gourma (Afrique occidentale); un ‘seuil’ et un bassin du précambrien supérieur; stratigraphie, tectonique, métamorphisme. Mémoires du B.R.G.M., 53, p 213
- Roddaz M, Debat P, Nikiema S (2007) Geochemistry of upper Birimian sediments (major and trace elements and Nd-Sr isotopes) and implications for weathering and tectonic setting of the Late Paleoproterozoic crust. *Prec Res* 159:197–211
- Rudnick RL (1995) Making continental-crust. *Nature* 378:571–578
- Salters VJM, Stracke A (2004) Composition of the depleted mantle. *Geochem Geophys Geosys* 5:Q05B07
- Sato K, Santosh M, Tsunogae T, Chetty TRK, Hirata T (2011) Subduction-accretion-collision history along the Gondwana suture in southern India: a laser ablation ICP-MS study of zircon chronology. *J Asian Earth Sci* 40:162–171
- Schmidt MW (1992) Amphibole composition in tonalite as a function of pressure—an experimental calibration of the Al-in-hornblende barometer. *Contrib Miner Petrol* 110:304–310
- Stern RJ (1994) Arc assembly and continental collision in the Neoproterozoic East African Orogen: implications for the consolidation of Gondwanaland. *Ann Rev Earth Planet Sci* 22:319–351
- Stern RJ (2010) The anatomy and ontogeny of modern intra-oceanic arc systems. *Geol Soc Lond Spec Publications* 338:7–34
- Stern RJ, Johnson P (2010) Continental lithosphere of the Arabian plate: a geologic, petrologic, and geophysical synthesis. *Earth Sci Rev* 101:29–67
- Stern RJ, Fouch MJ, Klempner S (2003). An overview of the Izu-Bonin-Mariana subduction factory. In: Eiler J, Hirschmann M (eds) Inside the subduction factory. Geophysical monograph, 138. American Geophysical Union, pp 175–222
- Straub SM, Goldstein SL, Class C, Schmidt A, Gomez-Tuena A (2010) Slab and mantle controls on the Sr-Nd-Pb-Hf isotope evolution of the post 42 Ma Izu-Bonin volcanic arc. *J Petrol* 51:993–1026

- Suyehiro K, Takahashi N, Ariie Y, Yokoi Y, Hino R, Shinohara M, Kanazawa T, Hirata N, Tokuyama H, Taira A (1996) Continental crust, crustal underplating, and low-Q upper mantle beneath an oceanic island arc. *Science* 272:390–392
- Takahashi N, Kodaira S, Tatsumi Y, Kaneda Y, Suyehiro K (2008) Structure and growth of the Izu-Bonin-Mariana arc crust: 1. Seismic constraint on crust and mantle structure of the Mariana arc-back-arc system. *J Geophys Res Solid Earth* 113:B01104
- Tatsumi Y, Shukuno H, Tani K, Takahashi N, Kodaira S, Kogiso T (2008) Structure and growth of the Izu-Bonin-Mariana arc crust: 2. Role of crust-mantle transformation and the transparent Moho in arc crust evolution. *J Geophys Res Solid Earth* 113:B02203
- Taylor SR, McLennan SM (1985) The continental crust: its composition and evolution. Blackwell, Oxford
- Thomas RJ, Fekkak A, Ennih N, Errami E, Loughlin SC, Gresse PG, Chevallier LP, Liégeois JP (2004) A new lithostratigraphic framework for the Anti-Atlas Orogen, Morocco. *J Afr Earth Sci* 39:217–226
- Will T, Okrusch M, Schmadicke E, Chen GL (1998) Phase relations in the greenschist-blueschist-amphibolite-eclogite facies in the system Na₂O-CaO-FeO-MgO-Al₂O₃-SiO₂-H₂O (NCFMASH), with application to metamorphic rocks from Samos, Greece. *Contrib Miner Petrol* 132:85–102
- Wood BJ, Turner SP (2009) Origin of primitive high-Mg andesite: constraints from natural examples and experiments. *Earth Planet Sci Lett* 283:59–66
- Yamamoto H, Yoshino T (1998) Superposition of replacements in the mafic granulites of the Jijal complex of the Kohistan arc, northern Pakistan: dehydration and rehydration within deep arc crust. *Lithos* 43:219–234
- Yoshino T, Okudaira T (2004) Crustal growth by magmatic accretion constrained by metamorphic P-T paths and thermal models of the Kohistan arc, NW Himalayas. *J Petrol* 45:2287–2302